Development of a Multipurpose Light Source for SiPM Characterization

von

Tim Enzweiler

Masterarbeit in Physik

vorgelegt der

Fakultät für Mathematik, Informatik und
Naturwissenschaften der RWTH Aachen

im November 2013

angefertigt am

III. Physikalischen Institut A

bei

Prof. Dr. Thomas Hebbeker

Gutachter und Betreuer

Prof. Dr. Thomas Hebbeker
III. Physikalisches Institut A
RWTH Aachen

Zweitgutachter

PD Dr. Oliver Pooth
III. Physikalisches Institut B
RWTH Aachen

Abstract

This thesis deals with the development and initial operation of a multipurpose light source for silicon photomultiplier (SiPM) characterizations. SiPMs are light-detectors for the detection of smallest amounts of light down to single photons. The presented light source is optimized for the measurement of the photon detection efficiency over a broad spectrum even in the UV-range. For this the lightsource has to provide a constant light flux as well as extremely short light pulses with a length of a few nanoseconds. In order to cover the whole dynamic range of a typical SiPM the light intensity should be adjustable from single photons up to serveral thousand photons per approximately 10 ns and square millimetre. The thesis describes design, operation and performance of the light source and its components. The latter is documented on the basis of several measurements with a reference detector. To take these measurements the reference detector has been comprehensively characterized, too.

Zusammenfassung

Diese Arbeit behandelt die Entwicklung und Inbetriebnahme einer Multifunktions-lichtquelle zur Charakterisierung von Silizium-Photomultipliern (SiPMs). SiPMs sind Lichtdetektoren zum Nachweis kleinster Lichtmengen von nur wenigen bis hin zu einzelnen Photonen. Die vorgestellte Lichtquelle ist optimiert für Messungen der Photonen-Nachweiswahrscheinlichkeit über ein breites Spektrum bis in den UV-Bereich. Hierfür muss die Lichtquelle sowohl einen konstanten Lichtstrom als auch extrem kurze Lichtpulse mit einer Länge von wenigen Nanosekunden bereitstellen. Die Lichtmenge soll dabei einstellbar sein und von einzelnen Photonen bis hin zu mehreren Tausend Photonen pro ca. 10 ns und Quadratmillimeter reichen, um den kompletten Dynamikbereich eines typischen SiPMs abzudecken. Die Arbeit beschreibt Design, Einsatzweise und Performance der Lichtquelle und ihrer Komponenten. Letztere wird anhand zahlreicher Messungen mit einem Referenzdetektor belegt. Um diese Messungen durchführen zu können, wurde auch eine umfangreiche Charakterisierung des Referenzdetektors durchgeführt.

Contents

1 Silicon Photomultipliers

Ever since the beginning of science, the detection of light has been of huge interest for physicists. Already Galilei used a telescope to observe light from distant stars, but at that time he used his eyes for light detection. For a long time, the human eye had been the best photodetector available. Some physicists even went so far as to take poisonous strychnine to enhance the sensitivity of their eyes.

Luckily, today's possibilities are more effective and less hazardous. The photocell, which was invented by H. Geitel and J. Elster in 1893, was the first electronic photo detector. It is based on the photoelectric effect which is also used for the photomultiplier tube (PMT). The PMT is an advancement of the photocell. It basically is a photocell with an electron multiplier.

With the upcoming of semiconductors, the invention of the photodiode established a new method of photon detection. It is a much smaller device and only needs a supply voltage of a few Volts. Ever since then all further improvements have been based on this technology. The silicon photomultipliers (SiPMs) are the latest invention in this field [1].

They are fast and very photosensitive detectors and are able to detect smallest amounts of light down to single photons. This makes them exceedingly useful for particle and astro-particle physics experiments.

Often SiPMs are used instead of classical photomultipliers since they offer several advantages. One asset is that a SiPM does not need a high supply voltage of several kV. The bias-voltage for a SiPM is typically only a few tens of Volts. In addition they are much smaller than normal photomultipliers (See fig.1.1) This in turn makes them a handy tool in light detection. Another big advantage towards PMTs is that they are not affected by high magnetic fields [2]. This fact makes them very interesting, especially for particle accelerator physics.

All in all one might say that SiPMs will play a major role in future physics experiments. For some experiments this future has already begun, they successfully profit from the use of SiPMs. The 'First G-APD Cherenkov Telescope' (FACT) observes active galactic nuclei. It measures cherenkov light with G-APDs [3]. These G-APDs are very similar to SiPMs, which basically consist of an array of G-APDs.

One of the first particle physics experiments which uses SiPMs in a detector is T2K. It uses SiPMs for the scintillator readout in the 'Pi-Zero subdetector' which measures the relevant cross section for neutrino interactions that generate π^0s. This is import-
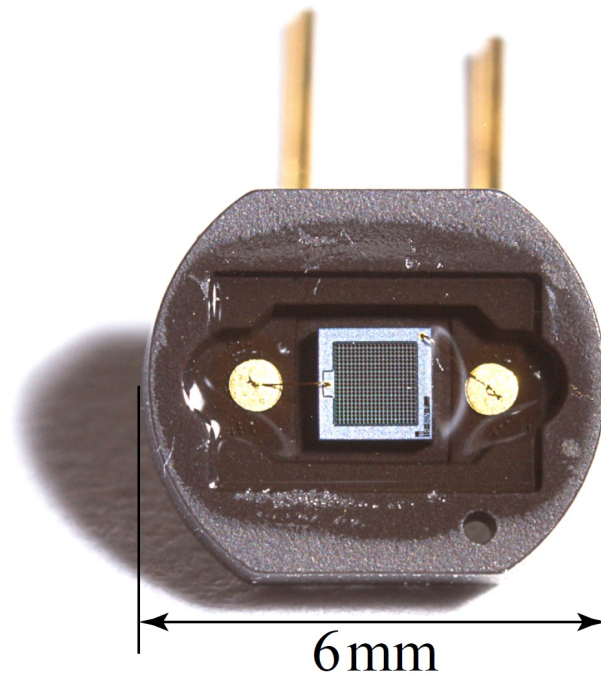
Figure 1.1: Silicon Photomultiplier (Model: Hamamatsu S10362-11-050C) with 400 pixels and an active area of $1\,mm^2$ (Photo: Benjamin Glauß, 2012)

ant because neutral current π^0 interactions present one of the dominant background sources in T2K [4].

A dark matter experiment that plans to use SiPMs is the XENON dark matter project. Among others the high single-photon detection efficiency in the UV regime (178 nm for Xenon) and the low bias voltages make SiPMs an attractive alternative to photomultiplier tubes for them [5].

The Physics Institute IIIA of the RWTH Aachen university also does some interesting research in the field of SiPMs and their applications. In astro-particle physics for example, FAMOUS[1] is a design study for the measurement of ultra-high-energy cosmic rays. It's a refracting telescope instrumented with SiPMs which measures the fluorescence light emitted by ultra-high-energy cosmic ray air showers [6].

An experiment that measures the cosmic ray positron fraction is the Positron Electron Balloon Spectrometer (PEBS). Here SiPMs are used for the tracking detector readout [7].

Moreover, big particle physics experiments like CMS are already using SiPMs and are currently planning to include SiPM in upcoming updates. The Velocity Drift Chamber system continuously measures the drift velocity for the CMS gas detectors. It successfully uses SiPMs to trigger the start of the drift time measurement [8]. The

---

[1]First Auger Multi-pixel-photon-counter-camera for the Observation of ultra-high-energy cosmic ray air Showers

outer hadron calorimeter is also being updated with SiPMs in the ongoing shutdown in 2013/2014. Here SiPMs are used for scintillator read out instead of hybrid-photo-diodes. Furthermore there are considerations of using SiPMs in a new fast muon trigger system called 'Muon track fast tag'. It would be located in the area of the present outer hadron calorimeter. Here SiPMs would be used to read out an array of scintillators with high granularity. In general high-energy particle physics experiments like the CMS detector also require the radiation hardness of SiPMs [9].

1.1 From pn-junction to Silicon Photomultiplier

A SiPM is an array of avalanche photodiodes operating in Geiger mode. In order to understand how SiPMs work, it is worthwhile to have a look at the photodiode and the avalanche photodiode first.

1.1.1 Photo Diode

A photodiode is basically a pn-junction which is exposed to light. In the pn-junction electrons from the n-doped region recombine with holes in the p-doped region and vice versa. Thus an electric field appears through the pn-junction. It can be enlarged by applying an external bias voltage. Photons incident to the pn-junction are able to generate electron-hole pairs. These electron-hole pairs are separated by the electric field as depicted in fig. 1.2. Thus a current can be measured between cathode and anode.

The performance of a photo diode is wavelength-dependent and can be characterized by its quantum efficiency which is the ratio of converted electrons to incident photons. This quantum efficiency is closely correlated to the 'responsivity' which describes the photocurrent (in ampere) per optical input power (in watt) [10]:

$$\mathscr{R} = \frac{I_{ph}}{P_{opt}} = \frac{\eta q}{h\nu} = \eta \frac{\lambda}{1.24\,\mu\mathrm{m}}\frac{\mathrm{A}}{\mathrm{W}} \tag{1.1}$$

with the elementary charge q, the frequency of the optical signal ν, the Planck constant h and the quantum efficiency η, which is the number of electron-hole pairs produced per photon.

The responsivity is an important property when using a photo diode as a reference detector for SiPM characterization. A rough calculation will give an impression of the needed accuracy for the measurement of the photocurrent: A SiPM is a single photon sensitive device. This means that one photon per $1\,\mathrm{mm}^2$ and light pulse is

a good assumption for the light flux. Furthermore choosing a wavelength of $400\,\mathrm{nm}$ and a pulse frequency of $50\,\mathrm{kHz}$ leads to a power of approximately $25\,\frac{\mathrm{fW}}{\mathrm{mm}^2}$. For a photo-detector with a sensitive area of $25\,\mathrm{mm}^2$ and a quantum efficiency of 80% equation 1.1 yields around $160\,\mathrm{fA}$. This is definitely a very small current to measure. Later in this thesis (in chapter 2) one will read about a SiPM teststand which uses a sourcemeter to measure a photocurrent. This sourcemeter (Keithley 2614b) has an accuracy of $100\,\mathrm{fA}$. In order to measure a signal much higher than the accuracy of the current measurement an optical attenuator can be installed in front of the SiPM. So the reference detector measures a higher signal than the SiPM. The ratio between the signals will be given by the attenuator.
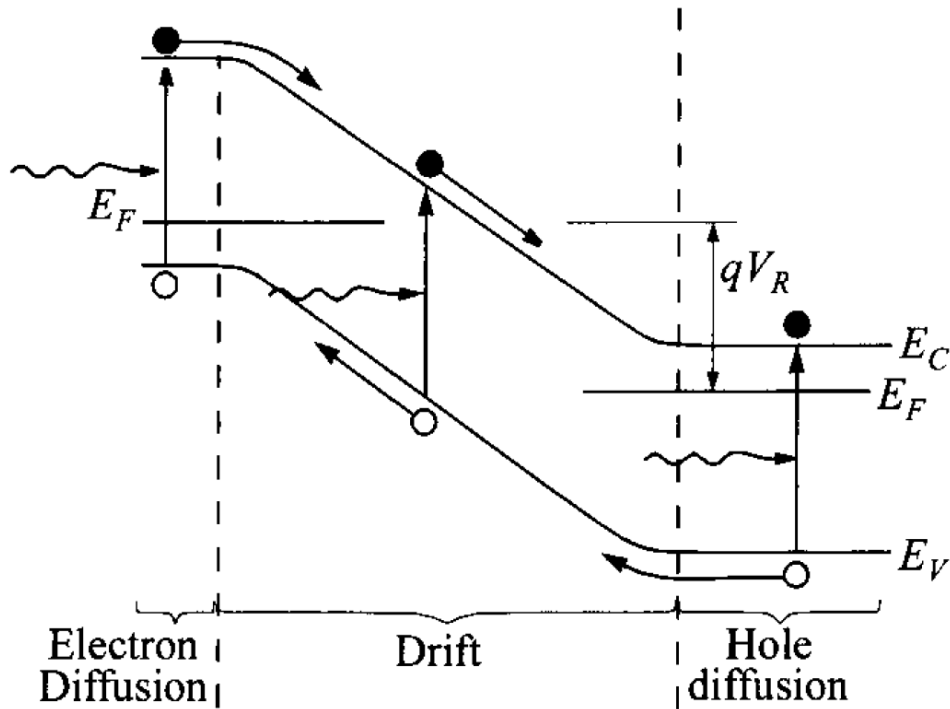

Figure 1.2: Energy-band diagram of a photodiode's pn-junction [10]. The electrons (black dots) and holes (white dots) are separated by the electric field.

1.1.2 Avalanche Photo Diode

The APD is a photo diode which is operated above the breakdown voltage. This means that the reverse voltage is so high that a photo-generated electron gains enough kinetic energy to free another bound electron. This electron again can produce another electron-hole pair. In this way, a single photon can trigger an avalanche breakdown with up to 10^4 charge carriers [10]. Fig. 1.3 shows this avalanche process.
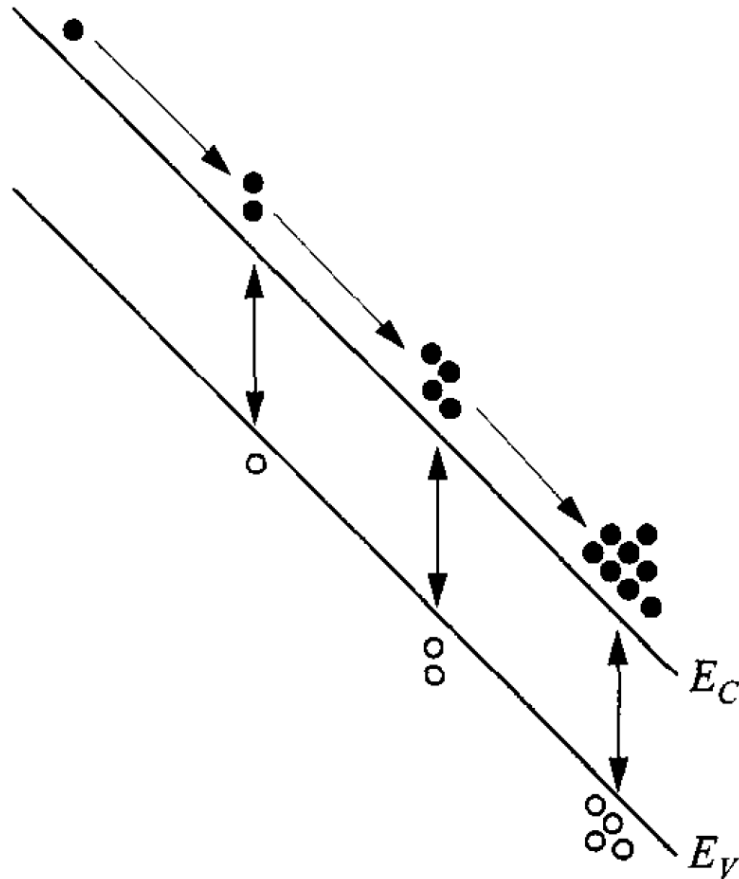
Figure 1.3: Sketch of an electron avalanche in a pn-junction. The electrons are depicted as points in the conduction band and the holes as circles in the valence band. The electrons get accelerated by the electric field and collide with electrons in the valence band. This releases additional electrons which then can also contribute to the avalanche. The created holes are more inert and so do not contribute to the chain reaction in this picture. Taken from [10].

The avalanche trigger probability for electrons P_e (and holes P_h) depends on the position of the charge carrier generation in the pn-junction. Fig. 1.4 shows that the avalanche trigger probability for electrons is highest near the p-edge of the pn-junction. The photon absorption length in silicon, and thus the position of charge carrier generation, is a function of its wavelength. This means that the design of the pn-junction determines at which wavelength range the diode works best.

The holes are more inert and hence need a higher reverse voltage to generate electron-hole pairs. This mode of operation where also the holes can start an avalanche, is called Geiger mode. Due to the opposite charge of the minority charge carrier it starts an avalanche in the other direction than the electron. This leads to a steadily increasing current. After a fraction of a nanosecond the whole Geiger mode APD (G-APD) becomes conductive. The current would become higher until the destruction of the

semiconductor. In order to avoid this, the avalanche breakdown has to be stopped. Here, one method is passive quenching by a resistor which is put in series with the G-APD. When the current rises the voltage then mainly drops over the resistor. In consequence of this, the voltage over the diode drops below the breakdown voltage and the avalanche stops.
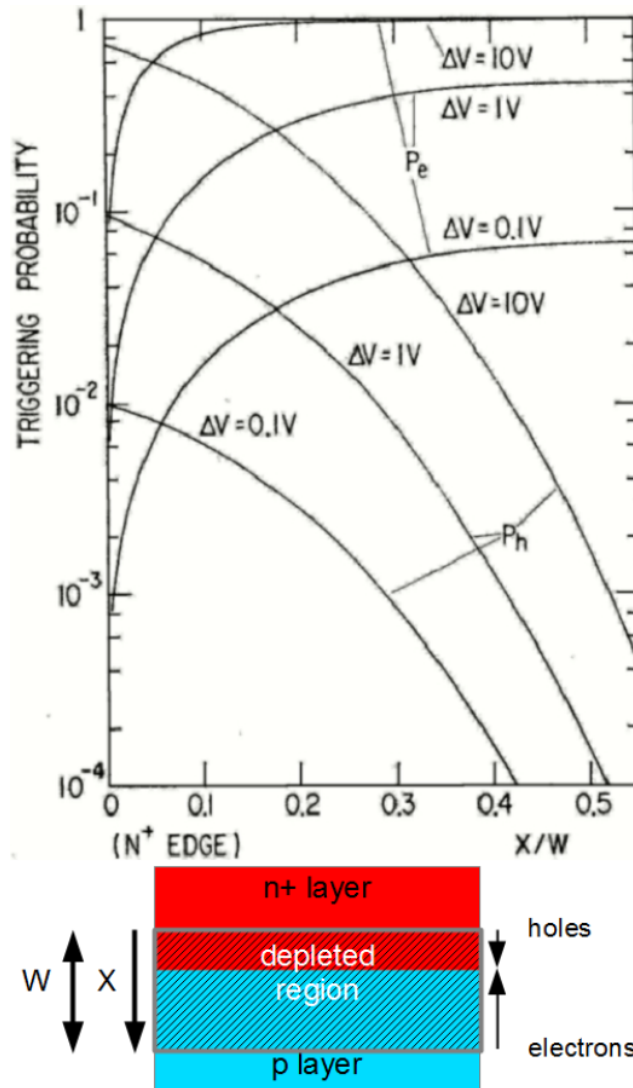

Figure 1.4: Avalanche trigger probabilities for electrons P_e and electron holes P_h at different bias voltages as a function of the position of the charge carrier pair's generation. The scheme at the bottom defines the position in the pn-junction. X is the depth within the depletion region beginning at the n-doped side. It is given as a fraction of the pn-junction's thickness W. Taken from [11], graph originally from [12]
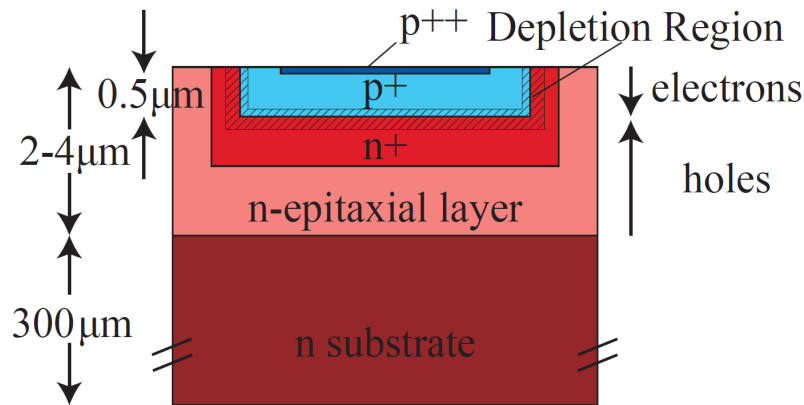
Figure 1.5: p on n type (G)-APD [13]

With this technique a single photon can be enough to produce a detectable signal. Otherwise there is no difference in the signal for one or more photons. This is due to the fact that once an avalanche breakdown is started the G-APD is 'blind' till it is quenched to its initial state.

The structure of an APD can be seen in fig. 1.5 [13]. The basis is formed by a $300\,\mu$m thick n-doped substrate. For production reasons there is a $2 - 4\,\mu$m n-doped epitaxial layer grown on top of it. The next layers are the heavily doped pn-junction. To achieve a uniformly distributed electric field within the pn-junction, there is an even higher doped p layer on top.

In a diode as described above light with a short absorption length generates electron-hole pairs at the p-doped side of the pn-junction. As one can see from fig. 1.6 this is light in the UV to blue range. Red light has a higher absorption length and so generates electron-hole pairs at the n-doped side of the pn-junction. When the charge carrier pair is created by blue light the electron and not the hole starts the avalanche. For red light the electron hole is used. Due to the fact that the avalanche trigger probability for electrons created in the p-doped region is higher than for electron holes created in the n-doped region this diode is optimized for short-wavelength light. An inverted structure with a p doped substrate and a n doped layer on top is used for more red sensitive devices.

The light absorption length in silicon is important for the diode's design. In order to understand the dramatic variation of the absorption length with the wavelength one has to consider that silicon has an indirect band gap of $1.1\,$eV. This means that the absorption of a photon by an electron always needs a phonon for momentum conservation. The needed momentum of this phonon decreases with an increasing photon energy. As the phonons underlie Bose-Einstein statistics there are more phonons with lower energy and thus the photon absorption is more probable. At a photon energy of $3.4\,$eV ($\sim 370\,$nm) the energy is large enough for a direct transition of the electron from the valence band to the conduction band.
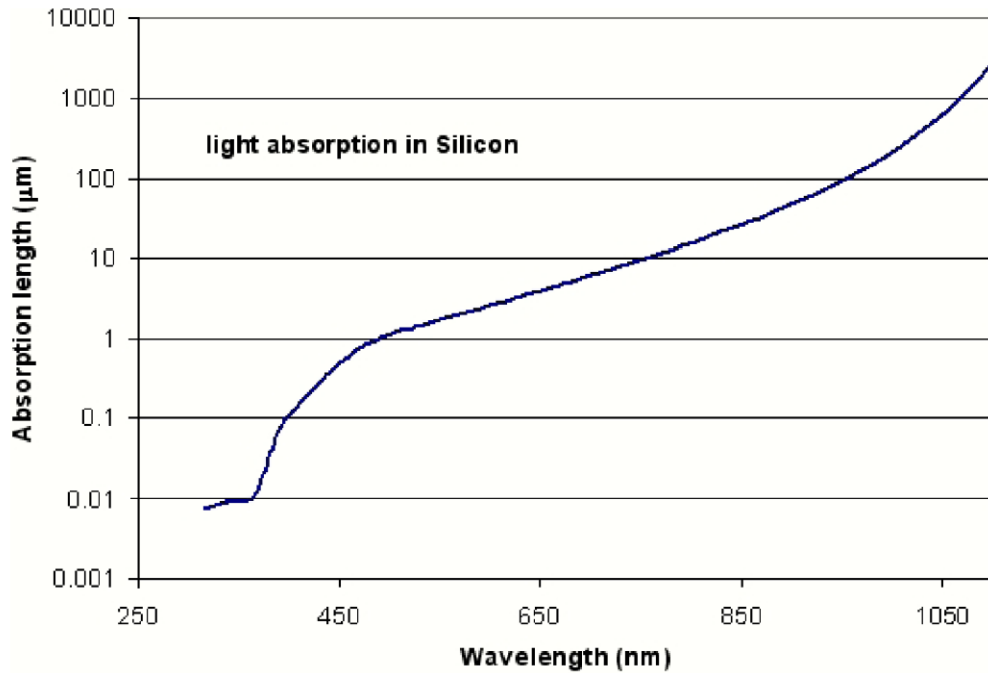
Figure 1.6: Light absorption length in silicon as a function of the wavelength. Taken
from [2], originally from [14]

1.1.3 Silicon Photo Multiplier

The G-APD described in chapter 1.1.2 has the advantage of a very high gain, but has
the disadvantage that it cannot distinguish between different numbers of photons.
This problem is solved by the SiPM. A Silicon photomultiplier is an array of G-
APDs (see fig. 1.7). The output signal is the analogue sum of the parallel connected
G-APDs. Since the G-APDs do not distinguish whether they are hit by one ore
more photons, the output signal increases not linear with the light flux. This is
demonstrated by a simulation which is shown in Fig. 1.8. A SiPM with 100 cells and
a photon detection efficiency of 50% needs about 800 photons at the same time for
99 cells to fire (under the assumption that the photons are equally distributed).

1.2 Properties of Silicon Photomultipliers

The SiPM's photon-detection-efficiency (pde) is

$$pde = \eta(\lambda) \times \epsilon_{Geiger} \times \epsilon_{geometry}, \tag{1.2}$$

where η is the wavelength dependent quantum efficiency. The Geiger discharge prob-
ability ϵ_{Geiger} is the probability that a generated electron-hole pair triggers an ava-

lanche breakdown and $\epsilon_{geometry}$ is the geometric fill factor. The fill factor describes the fact that not the whole SiPM's surface is a sensitive area. The fill factor typically varies between 30% and 80%. The space between the cells is needed to separate the cells from each other. Some space is also taken by the quenching resistors and wires. In the next three sections one can read about effects of thermal noise and correlated noise (afterpulsing and optical crosstalk) that let the pde appear higher than it actually is.
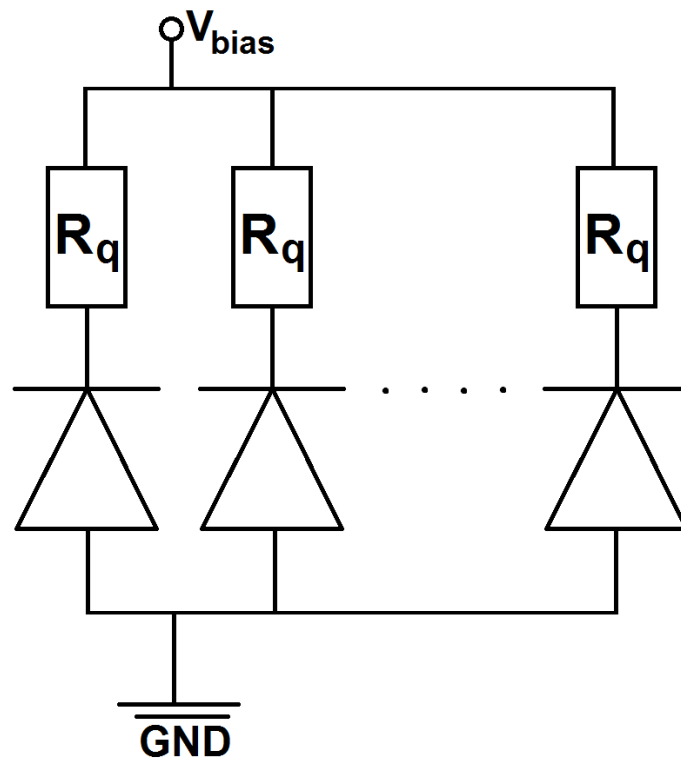

Figure 1.7: Circuit scheme of a Silicon photomultiplier: The output signal is the analogue sum of the parallel connected G-APDs.
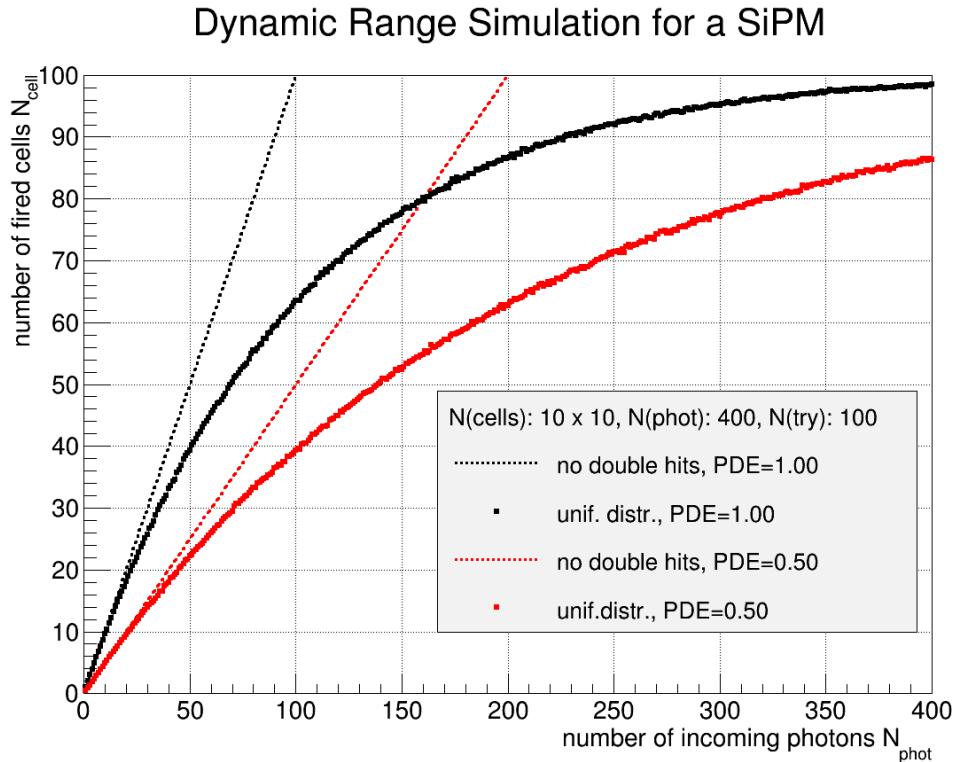
Figure 1.8: Simulation of the dynamic range of an SiPM with 100 cells. The colour indicates the assumed photon detection efficiency (pde) (see chapter 1.2). Black would be an ideal SiPM, against what red represents a realistic SiPM. The dashed lines show what the output signal would be if every cell was hit by no more than one photon. In reality double hits are common and the number of fired cells is much lower. The continuous lines show this expected number of fired cells. Adapted from [15]

.

1.2.1 Thermal Noise

Electron-hole pairs cannot only be created by photons but also by thermal excitation. When so induced charge carriers trigger an avalanche breakdown, the signal is indistinguishable from that of a photon generated one. This effect is called thermal noise. For a good pde measurement this thermal noise has to be subtracted. This in turn means that dark measurements have to be done. As the thermal noise is expected to vary with the temperature, these measurements have to be done at the same temperature as the pde measurement.

1.2.2 Afterpulsing

During an avalanche breakdown charge carriers can be excited to a metastable state at a higher energy level. These metastable state can have a lifetime of tens of ns,

long enough to survive until the initial avalanche breakdown is stopped. This means that the excited charge carrier is able to start an additional avalanche breakdown. This phenomenon called afterpulsing occurs due to impurities in the silicon lattice. The afterpulses are not distinguishable from pulses triggered by a light signal. This makes it necessary to also know the afterpulse probability when measuring the pde. In order to investigate this afterpulse probability one possibility is to measure the distribution of the time between the events. Due to the uniform distribution of the thermal noise the time difference between two noise events is supposed to be distributed exponentially. Adding one or two exponential distributions for the afterpulsing leads to a superposition of exponential functions. Fitting this function to the measured distribution eventually leads to the afterpulsing probability (see table 7.1 in [11]).

1.2.3 Optical Crosstalk

Optical crosstalk is an effect where photons emitted within the SiPM trigger an avalanche breakdown. These photons can be emitted via charge carrier multiplication. They either directly trigger another cell or first get absorbed and then re-emitted in the epitaxial layer or in the substrate below. The direct optical crosstalk can be reduced with optical trenches between the cells.

The optical crosstalk has to be considered when measuring the pde. One possibility of determining the crosstalk probability is to do a dark measurement where only thermal noise is expected. This means that nearly every event where two or more cells fire are crosstalk events. (Measured by [11])

For all the applications which were introduced at the beginning of this chapter it is crucial to understand and measure the characteristics of SiPMs. One of the most interesting SiPM properties to investigate is the photon-detection-efficiency. As one can read in chapter 1.2 this means that afterpulsing and optical cross-talk become very important characteristics as well. All these characteristics must be studied in dependency of temperature and overvoltage. Furthermore it is worthwhile to characterize SiPMs over a huge dynamic range.

2 The extended SiPM Test Stand

As mentioned in chapter. 1 there are several characteristics of SiPMs which are worthwhile to look at. For this purpose the Physics Institute IIIA of the RWTH Aachen university has developed a SiPM teststand. It is designed to measure the pde of SiPMs in dependency of temperature and overvoltage over a huge dynamic range fully automated.

The initial idea for the SiPM test stand [16] including a tunable light source [17] was presented in 2010. The initial state of the teststand [13] at the beginning of this thesis work is depicted in fig. 2.1. In this version two different light sources were used. First, a white light LED (*Cree* CXA2011) in conjunction with a monochromator was employed. This provides a constant light flux with a wavelength which can be chosen from a wide spectral range. Second, a set of seven monochromatic LEDs was built. These were separately pulsed with a function generator (AFG3252). Due to the limited power of the function generator (+5 V output voltage) the light output was limited as well. The light from either the white light or a monochromatic LED was concentrated with an acrylic cone and coupled into an optical fibre. In the case of using the white light LED this fibre led to a monochromator.

This monochromator was realised with a blazed grating. The white light was fanned out and picked up by another fibre mounted on a motorized stage. This fibre then led to an integrating sphere. The SiPM and the reference detector were connected to this integrating sphere. As a reference detector a PIN diode (Hamamatsu S9195 [18]) was used. In order to measure the generated current, it was connected to a picoammeter (Keithley Model 6485 [19]).

2.1 The Modified Optical Design

Some parts of the SiPM teststand which is described above have now been modified: Instead of an integrating sphere two beam splitters are used. The integrating sphere has the disadvantage that due to multiple reflections at its walls it stretches the light pulse. This can be demonstrated by a simple calculation:

Assuming that photons at the end of an incoming pulse get easily reflected up to a hundred times (port area is $\frac{1}{32}$'th of the whole area of the integrating sphere), the temporal elongation is given by

$$\frac{100 \cdot d}{c} \approx 17 \text{ns}, \tag{2.1}$$

where c is the speed of light and $d \approx 3$ cm the diameter of the integrating sphere. This means that any effort in generating short light pulses is useless as long as one uses an integrating sphere. This clearly disqualifies the integrating sphere for light pulses shorter than 10 ns. In addition the beam splitters have a better transmission than the integrating sphere. The used beam splitter (Thorlabs BS013) has a transmission of $\sim 50\%$ in the range from 400 nm to 700 nm as on can see in fig. 2.2. In the UV range the transmission drops down to zero, but is at least higher than 10% for all wavelengths bigger than approximately 325 nm. Since characterizing the SiPM's behaviour in the UV range is a very interesting topic, all components are optimized to be transmissive in that range. For this reason all optical fibres of the SiPM teststand have been changed to special solarization-resistant fibres with a diameter of 400 μm. The transmission of the used fibre (M22L01) is shown in fig. 2.3. Even in the UV range its transmission is higher than 90%.

A collimator is used to gather the light from the light source to the first optical fibre. The used F220SMA-A is aligned to the optical fibre for light with a wavelength ranging from 350 nm to 700 nm. To achieve an equally distributed light flux there are diffusers (ED1-C50-MD) mounted between the beam splitter and the SiPM/reference detector. This is important because the different SiPMs and the reference detector do not have the same light-sensitive area. The photo in fig. 2.4 gives a good impression of the light distribution. For the future it is planned to install an aperture with the size and shape of the sensitive area of the PIN diode and of the SiPM between the diffusor and the light detecting device. The aperture is designed in a way that only nearly parallel light will enter the sensitive area. The whole set up of the modified SiPM teststand is shown in fig. 2.5. The light emitted by the multipurpose light source is distributed to SiPM, PIN diode and spectrometer. The multipurpose light source has two light pick ups. One directly leads to the first beam splitter, the other optical path also includes the monochromator. This means, that the set-up does not need to be changed anymore to use the monochromator. The PIN diode is used as a reference detector. Comparing its signal with the SiPM's signal yields the pde. The spectrometer measures the spectrum of the light. Constantly monitoring the spectrum makes sense as the LED's spectrum depends on the temperature of the pn-junction. A higher junction temperature shifts the whole spectrum to longer wavelengths [20] (The shift is in the order of a few nm). With this set-up the pde can be measured precisely as a function of the wavelength.

The optical path is determined by optical fibres and two beam splitters which are connected to each other by a tube.
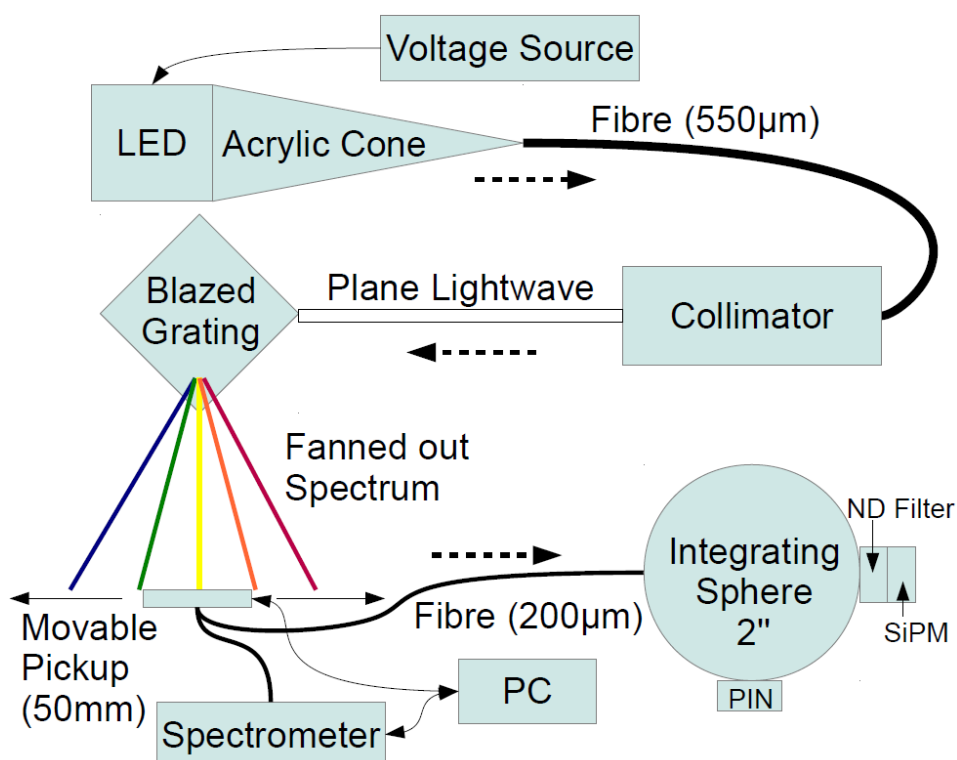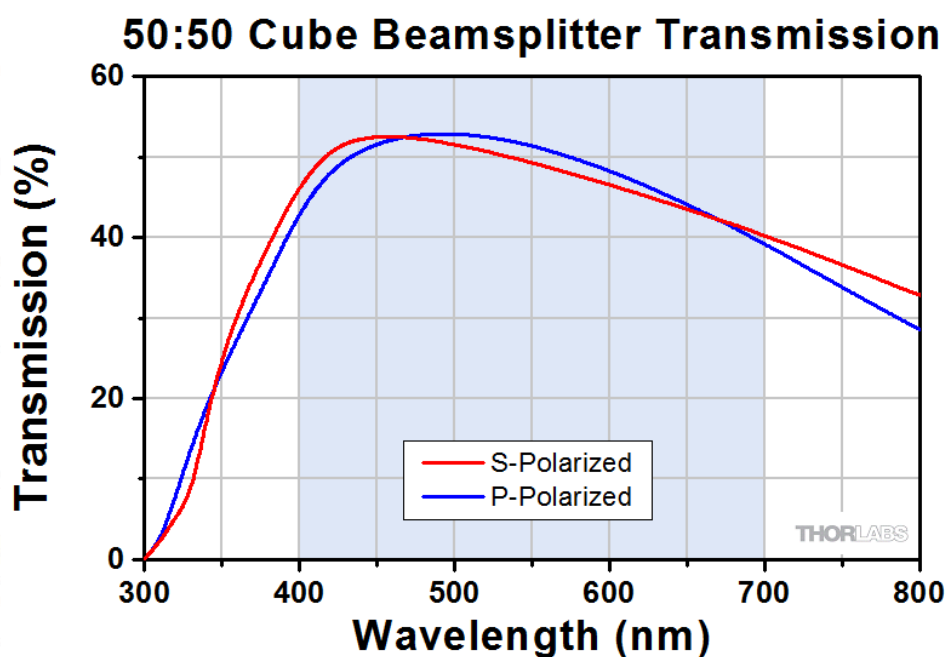
Figure 2.1: Sketch of the SiPM teststand in 2012 [13].

Figure 2.2: Transmission of the Thorlabs BS013 beam splitter. Taken from www.thorlabs.de
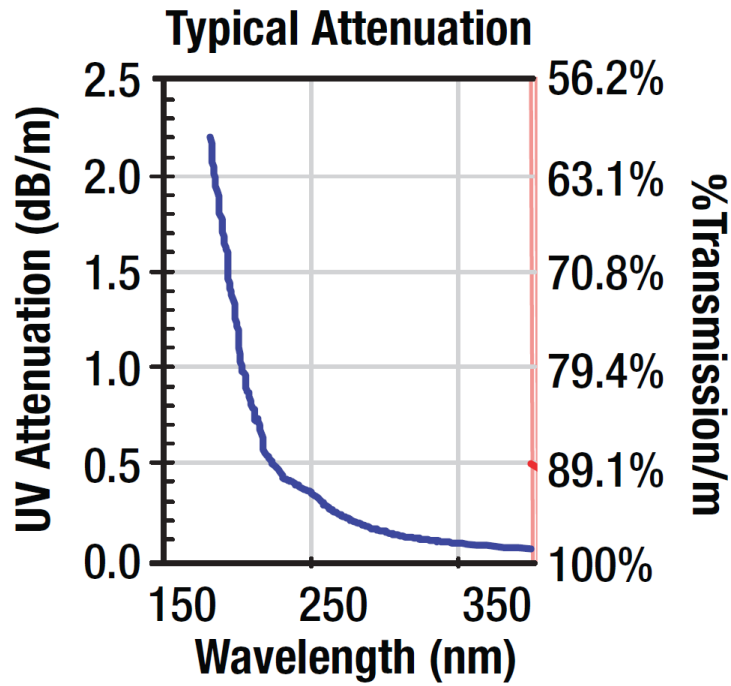
Figure 2.3: Transmission of the optical fibre M22L01. Taken from www.thorlabs.de
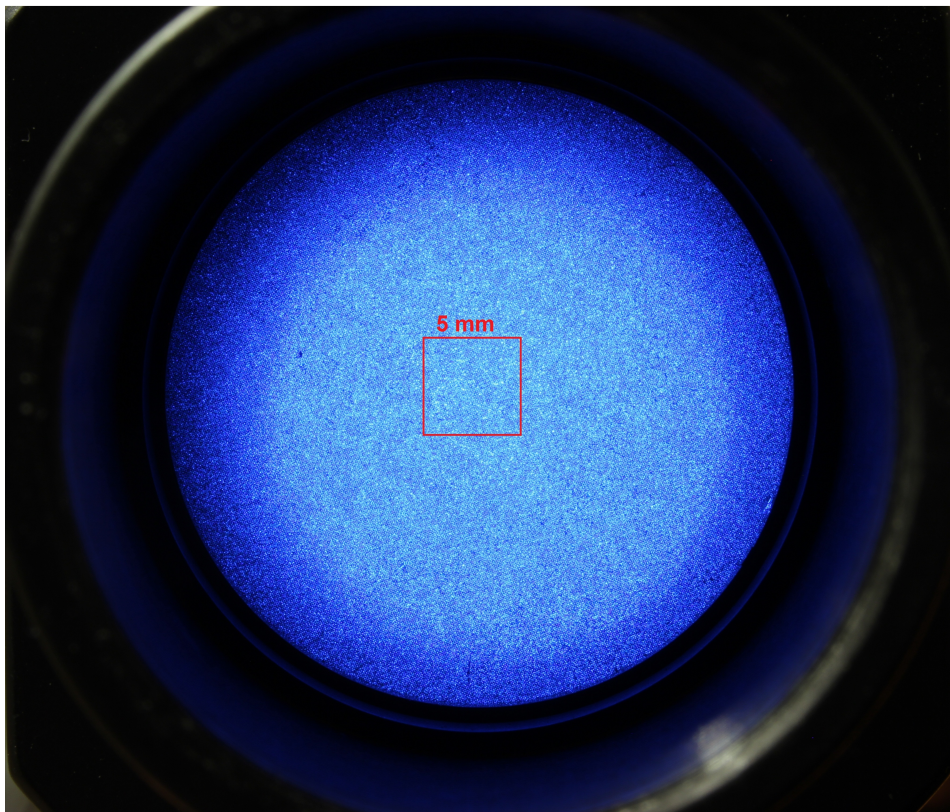

Figure 2.4: Photo of the diffuser's surface. The diffuser is used to achieve an equally
distributed light flux over the sensitive area of the SiPM or the PIN diode.
The read square with 5 mm edge length shows the size of the PIN diode's
sensitive area. The sensitive area's size of typical SiPMs is in the same
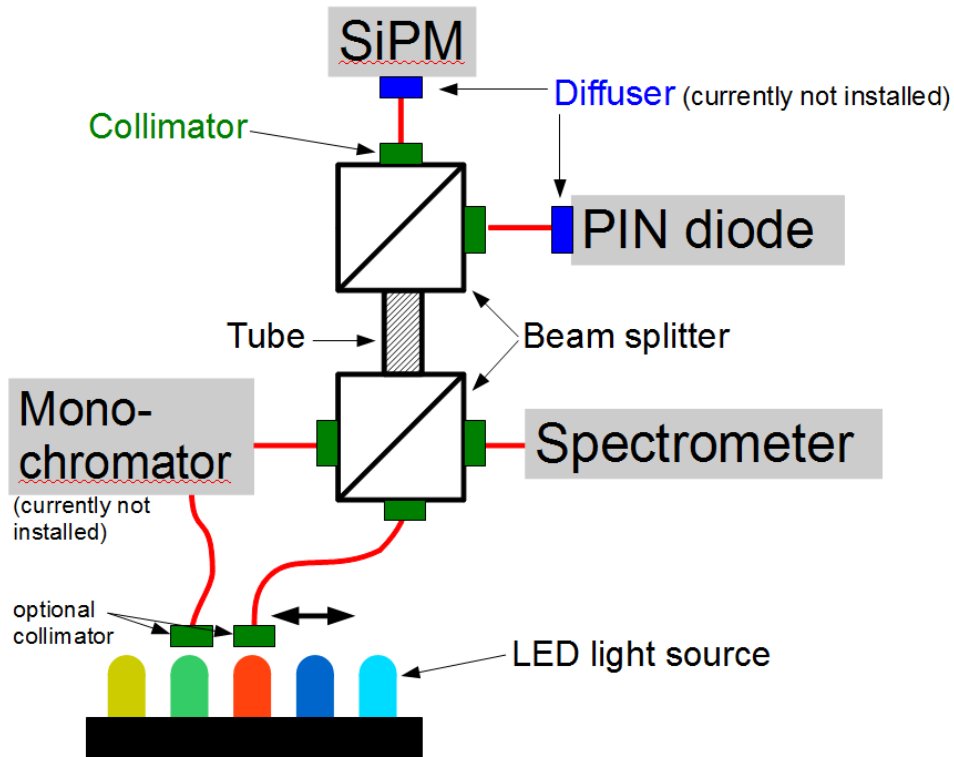order of magnitude

Figure 2.5: Sketch of the SiPM teststand in 2013

2.2 Measuring the pde

The pde is measured in two ways. A relative pde measurement compares the photon-detection-efficiency of the SiPM at different wavelengths to each other. Therefore multiple measurements at different wavelengths are made. For each measurement the SiPM signal is compared with the reference detector signal. Thus one obtains the pde in small steps over a huge spectrum. This relative pde is then scaled to a set of absolute pde measurements.

Measuring the absolute pde is a bit more tricky. One method is to exploit the fact that for a small number of events, according to poissonian statistics, the mean number of events μ is totally determined by the possibility for no event.

For the absolute pde measurement very short light pulses of only a few photons are used. The pulse length has to be shorter than the recovery time of the investigated SiPM. If these light pulses exist of only a few photons, one can apply poissonian statistics. This means that the probability to measure k photons is

$$p(k) = \frac{\mu^k \cdot e^{-\mu}}{k!}.$$

(2.2)

This implies that the probability to measure no photon is

$$p(0) = \frac{\mu^0 \cdot e^{-\mu}}{0!} = e^{-\mu}. \tag{2.3}$$

Its value is obtained by measuring the relation of number of measured pedestal photons N_{ped} and the total number of incident photons N_{tot}. This means that

$$p(0) = \frac{N_{ped}}{N_{tot}}. \tag{2.4}$$

Combining eqn. 2.3 and eqn. 2.4 yields

$$\mu = -\ln \frac{N_{ped}}{N_{tot}} \tag{2.5}$$

The so measured result μ_{light} has to be corrected by a dark measurement. Therefore the same measurement and calculation is done just without light pulses. The so obtained μ_{dark} is subtracted from the original measurement:

$$\mu_{corr} = \mu_{light} - \mu_{dark} \tag{2.6}$$

The pde is now obtained by dividing this corrected value μ_{corr} by the mean number of photons per pulse n_γ which is measured with the reference detector. So eventually

$$\text{pde} = \frac{\mu_{corr}}{n_\gamma}. \tag{2.7}$$

2.3 Requirements for the Light Source

The multipurpose light source is designed to do pde measurements with the SiPM teststand. This means it has to fulfil the requirements of relative and absolute pde measurements and allow the exploration of the dynamic range of SiPMs. The covered spectrum of the light source should reach from deep ultraviolet to red.

The light source has to provide a constant light flux for relative pde measurements as well as short light pulses for absolute pde measurements. Furthermore for the intensity of the light pulses and the constant light flux a huge dynamic range is favoured.

2.3.1 Pulser

The light pulse for the absolute pde measurement has to be shorter than the recovery time of the SiPM. Measurements of the recovery time of various SiPMs result in recovery times of more than 10ns [21]. This means a pulse length of less than 10ns would be good for all kinds of SiPMs. Another method to verify this time is to look at the electrical properties of a SiPM. If a breakdown occurs, the diode in first approximation reacts as a charging capacitor. This means that the recovery time is in the same order as the RC time constant:

$$\tau = R \cdot C \tag{2.8}$$

Impedance measurement of SiPMs mostly lead to recovery times longer than $10\,\mathrm{ns}$ as well [22].

Very good light sources for pulsing are LEDs and in order to get short light pulses one needs short electric pulses. LEDs are typically driven at about $30\,\mathrm{mA}$, but certain LEDs stand currents up to $1.5\,\mathrm{A}$. However, due to the extremely small duty-cycle much higher currents are possible for all kinds of LEDs. This means that the pulser should cover a huge dynamic range.

2.3.2 DC Source

For the constant light flux LEDs are suitable, too. Due to the specifications of the different LEDs the constant current source should provide a stable direct current of up to 1.5A. Also, a high precision in the sub-mA range is desirable.

3 Reference Detector

The reference detector has a great influence on the accuracy of the pde measurement.Therefore it is of vital importance to "improve" the reference detector system. It mainly consists of the PIN diode S9195 [18] (shown in fig. 3.1) and the Keithley Sourcemeter 2614b [23]. It supplies the PIN diode with bias voltage and measures the photocurrent at the same time.

Figure 3.1: S9195 PIN diode with a sensitive area of $5 \times 5 \, \mathrm{mm}^2$. Picture taken from [24]

3.1 PIN Diode

The PIN diode is similar to a PN diode. The 'I' in PIN diode stands for intrinsic. This means it has an intrinsic semiconductor region between the N-type and the P-type region. This enlarges the depletion region which is created by the P-N junction. A larger depletion region leads to a more stable measurement and a bigger wavelength range.

The PIN diode, like all diodes, always has a parasitic capacitance which cuts off high frequency signals. This capacitance is related to the size of the PIN diode's sensitive area. Nevertheless, the used PIN diode has a rather big sensitive area of $25 \, \mathrm{mm}^2$. This is important as SiPMs are able to detect smallest amounts of light and accordingly shall also be characterized with low light fluxes. The comparatively large area of the PIN diode is important to get a sufficiently high reference signal at low light fluxes. The used PIN diode has a terminal capacitance of $60 \, \mathrm{pF}$ and a cut-off frequency of 50MHz. Thus the measured current, and accordingly the photon flux, is always integrated over a certain time.

For the use as reference detector a high responsivity in the used spectral range is important. This is for the same reason as for the large sensitive area. The used PIN diode's spectral responsivity and quantum efficiency are shown in 3.2 and 3.3.

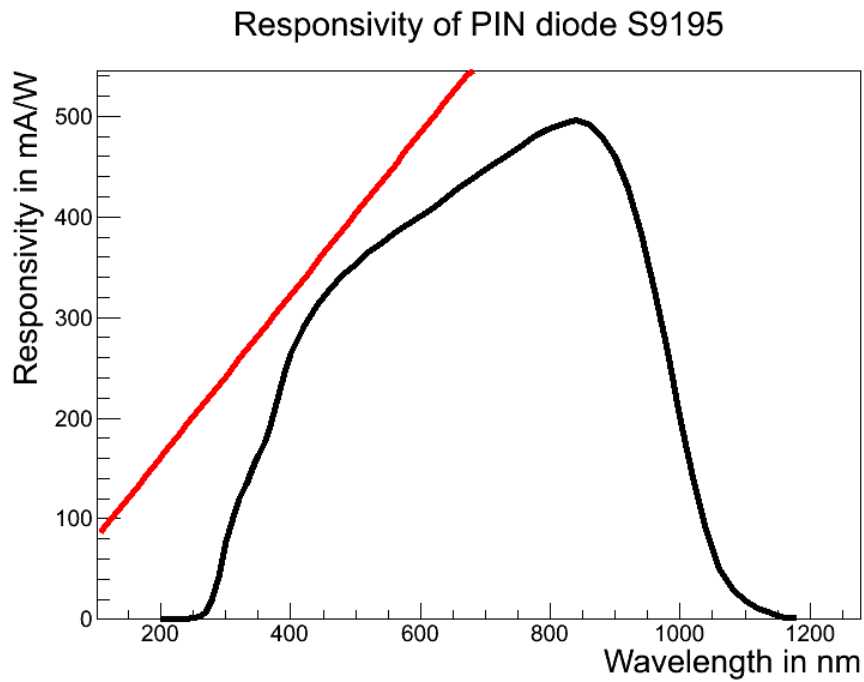Responsivity of PIN diode S9195

Figure 3.2: Responsivity of the used PIN diode (S9195) as calibrated by Hamamatsu. The red line corresponds to a quantum efficiency of 100%. Plotted with data from [25]
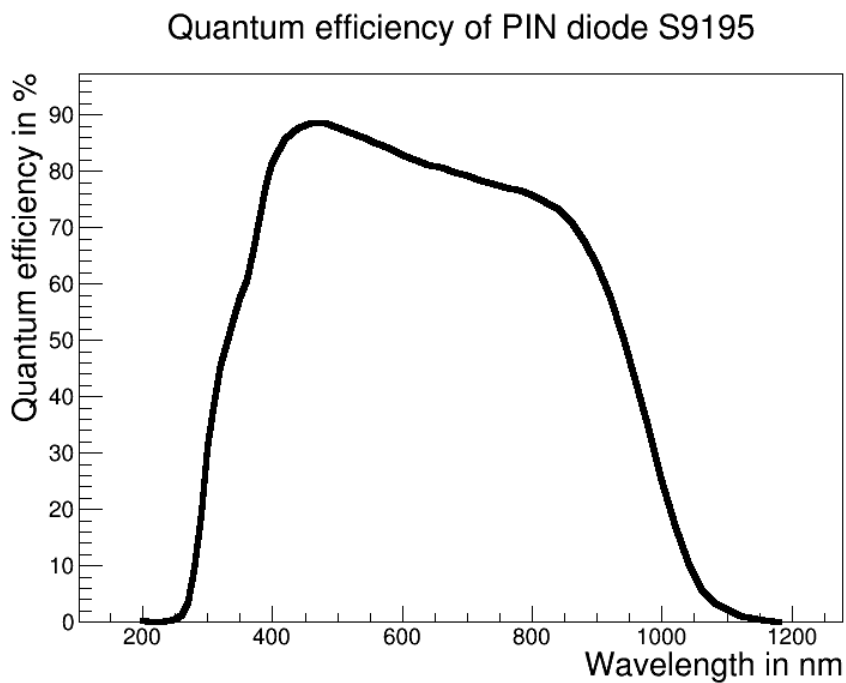
Quantum efficiency of PIN diode S9195

Figure 3.3: Quantum efficiency of the used PIN diode (S9195) as calibrated by Hamamatsu. Plotted with data from [25]

3.2 Low Current Measurements

Low (direct) current measurements are not trivial and there are a lot of effects that can influence the measurement. Naturally one has to avoid any kind of capacitive coupling of parasitic signals to the test circuit. Thus the PIN-diode and the connecting cable are totally surrounded by aluminium foil. What happens without shielding is shown in fig. 3.4. In this measurement one clearly sees the mains frequency of 50 Hz. One might say that if the measurement is significantly longer than the period the mean of the measurement is not changed by the periodic signal. This nevertheless shows how easily interference signals couple into the measurement circuit.
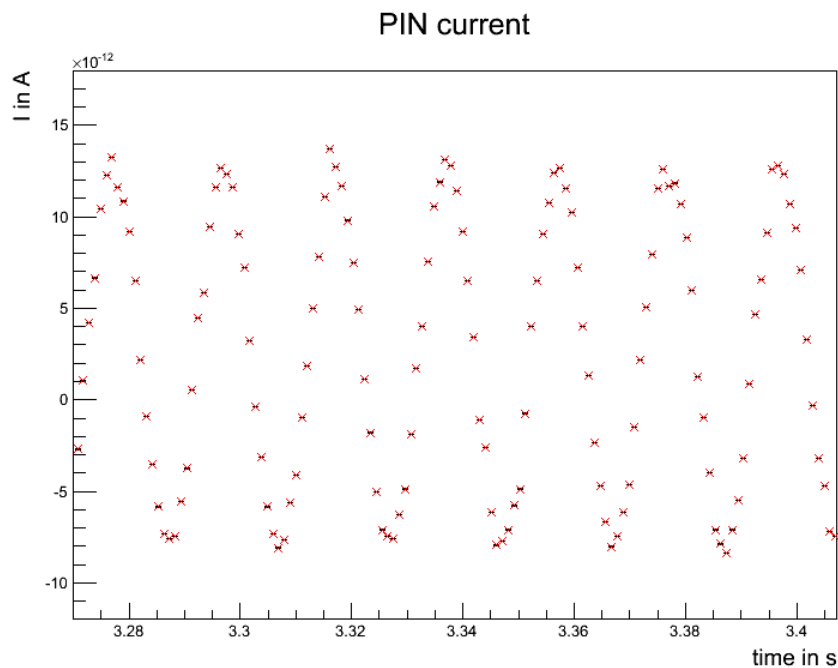

Figure 3.4: Measurement with unshielded PIN diode and cable. A huge interfering signal with a frequency of 50 Hz couples into the set-up.

Another problem is that when measuring currents in the pA range the residual resistance of insulators are no longer negligible. The potential difference between the inner core of the cable and outer sheath leads to an additional contribution in the measurement [26]. In order to avoid this one uses a triaxial cable as shown in fig. 3.5. An additional inner sheath called 'guard' is put at the same voltage as the bias voltage of the PIN-diode. Thus the source of the leakage current is moved from the force to the guard, and so out of the measurement circuit.

3.3 Bias Voltage of the PIN Diode

The PIN photodiode is reverse biased. Under reverse bias the diode does not conduct except for a small dark current. The bias voltage enlarges the depletion region of the PIN diode and hence the sensitive area for light detection. The depth of the depletion region is proportional to the square root of the bias voltage [10]. A higher bias voltage, however, in turn evokes the disadvantage of a higher dark current. For the used PIN diode the dark current is measured for different bias voltages from 0 to 15 Volt (at 24.5°C ambient temperature). The results can be seen in fig. 3.6. Looking at the dark current curve another advantage becomes visible. With higher bias voltage the dark current changes less with bias voltage variations. This leads to a more stable dark current level. For the measurements done in this chapter the bias voltage is set to $2\,$V.
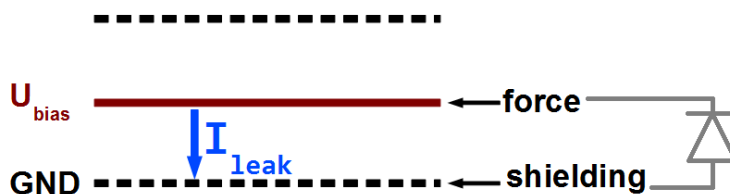
3.4 Dark Current Measurement

In order to characterize the reference detector a long-term dark current measurement is done. The PIN diode [18] is connected to the sourcemeter via RG58A/U triaxial cable as described in chapter 3.2. The cable length is kept short to avoid coupling of interfering signals. The whole measuring line from sourcemeter input to the PIN diode is completely shielded with aluminium foil. This shielding is connected to the sourcemeter housing. A DS18B20 temperature sensor is mounted near the set up to control the temperature profile.

The long term measurement consists of about 5000 measurements. An example is shown in fig. 3.7. Each of these measurements is done over $10\,$s and has 500 readings. Each of these readings is an integration over one power line cycle ($\frac{1}{50\,\mathrm{Hz}} = 20\,\mathrm{ms}$). The idea behind this is to keep interfering signals which enter the measurement circuit despite shielding at a constant level. Most interfering signals are emitted at $50\,$Hz. When integrating always over one period the coupling interfering signals end up in a constant systematic offset (independent of the phase).

The total time for one measurement is more than just the time for the readings, since there is some additional time needed for the data transfer. This means that one measurement takes about $50\,$s in total. The error for a single current measurement is 0.06% [23]. In order to avoid switch-on effects the first 100 readings ($\sim 2\,$s) are not analysed. According to the manufacturer there is an additional systematic uncertainty of $100\,$pA which is not considered here. This is no problem as one does not look at single measurements, but always subtracts a dark current measurement from a light measurement. As a result of this the systematic uncertainty is cancelled out. Furthermore, during all measurements the temperature is logged.

Coaxial cable

U_{bias}

I_{leak}

GND

force

shielding

Triaxial cable

U_{bias}

U_{bias}
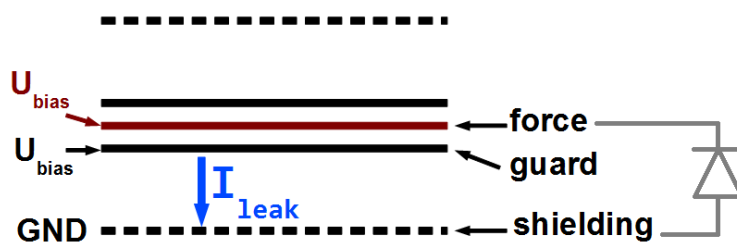
I_{leak}

GND

force

guard

shielding

Figure 3.5: Leakage current in coaxial and triaxial cable. The sourcemeter measures the current between force and ground. The triaxial cable has an additional sheath called guard, which is at the same potential as the force. Thus the source of the leakage current is moved from the force to the guard.
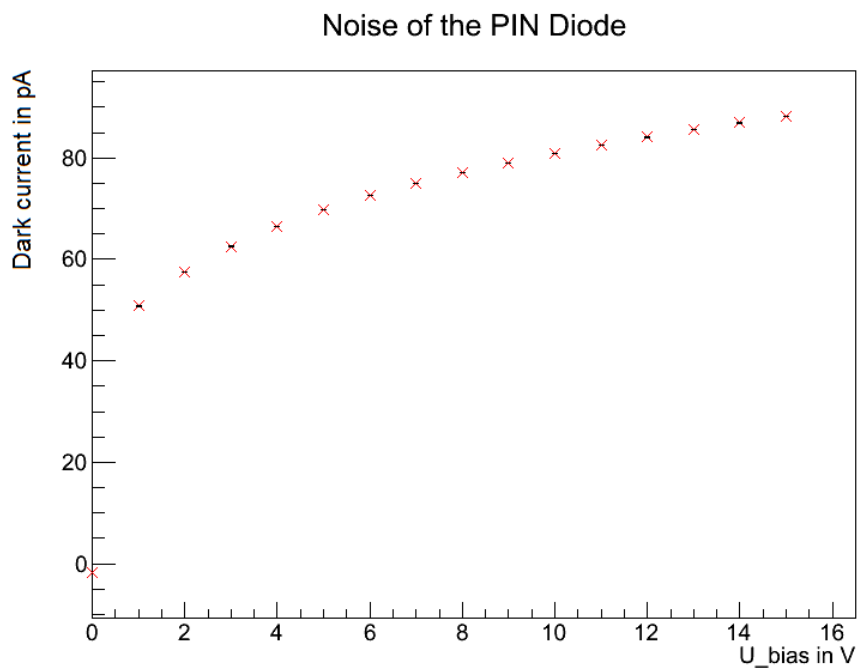
Noise of the PIN Diode

Figure 3.6: Noise of the PIN diode in dependence of the applied bias voltage.

For each measurement the recorded PIN currents are histogrammed like in fig. 3.8. As expected the readings are gaussianly distributed. Thus the mean of the gaussian fit is used as mean value of the measurement. In the example in fig. 3.8 the measured current is $58.6 \pm 0.04\,\mathrm{pA}$.

Analysing all measurements in such a way leads to a current profile as shown in fig. 3.9. Obviously the PIN current is strongly depending on the temperature. The temperature dependence of the current in a reverse biased pn-junction is given by [27]

$$I_{corrected} = I_{measured} \cdot e^{-c_T \Delta T} \tag{3.1}$$

with the temperature coefficient c_T and the temperature difference to a reference temperature ΔT. The chosen reference temperature of $25^{\circ}\mathrm{C}$ is also the temperature for which the PIN diode is calibrated. The temperature difference is averaged over five measurements, so that

$$\Delta T(n) = \frac{\sum\limits_{k=n+n_{\mathrm{offset}}-2}^{n+n_{\mathrm{offset}}+2} T(k)}{5} - 25^{\circ}\mathrm{C} \tag{3.2}$$

Here n refers to the respective measurement and n_{offset} respects the fact that the temperature sensor does not measure directly at the pn-junction but outside of the shielding. This means that a temperature change outside of the shielding causes a temperature change inside of the shielding with time delay. This time delay is represented by n_{offset} which multiplied by 50 (time for one measurement) yields the time delay in seconds. Applying this temperature correction leads to a temperature corrected current which is the reverse current at $25^{\circ}\mathrm{C}$, where the calibration of the PIN diode is done.

The temperature coefficient c_T and the offset n_{offset} are the open parameters of the temperature correction. The temperature coefficient is a property of the PIN diode which is not given by the manufacturer and the offset is a consequence of the PIN diode's shielding which thermally separates it from the temperature sensor. If these two parameters are chosen well, the temperature corrected current should be gaussian distributed like in fig. 3.10. In order to determine them, the temperature corrected current is calculated for different sets of c_T and n_{offset}. The χ^2/N_{dof} of the gauss fit to the histogrammed temperature corrected current is shown in fig. 3.11. Searching a region in which the χ^2/N_{dof} is minimal leads to $c_T = 0.14$ and $n_{\mathrm{offset}} = 38$ (this is equivalent to a time of $\sim 30\,\mathrm{min}$). Within a region of about $\pm 3\%$ for the temperature coefficient and $\pm 5\%$ for the offset the χ^2/N_{dof} is between one and two.
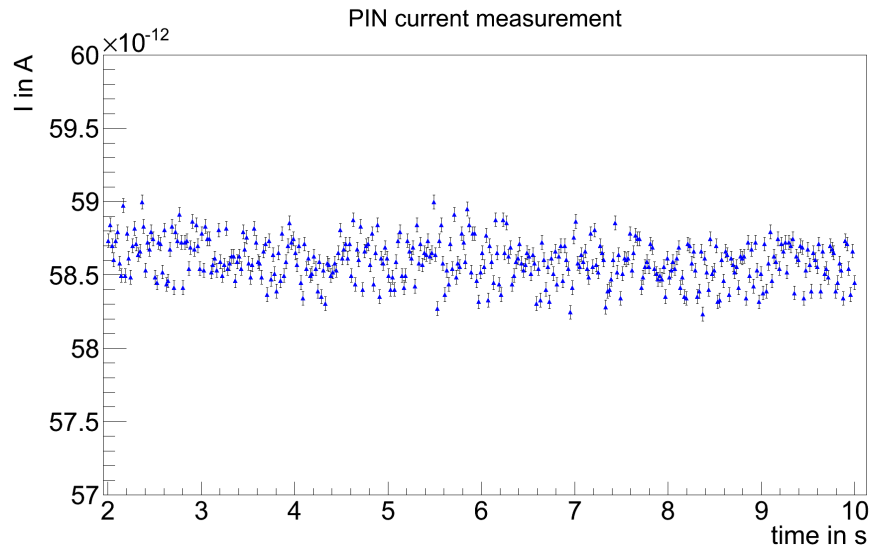
Figure 3.7: Typical dark current measured at the PIN diode. Each point represents an integration over one power-line-cycle. The data taken in the first two seconds is not used due to switch-on effects.
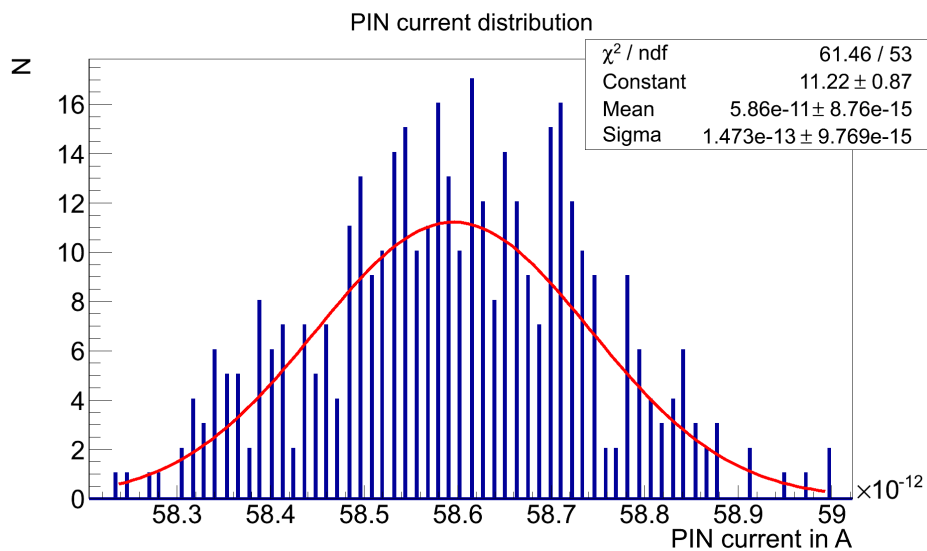

Figure 3.8: Distribution of the measured dark current shown in fig. 3.7. The mean value of the measurement is estimated by the mean of the fitted gaussian function. The χ^2/N_{dof} is in accordance with the assumption of a gaussian distribution.
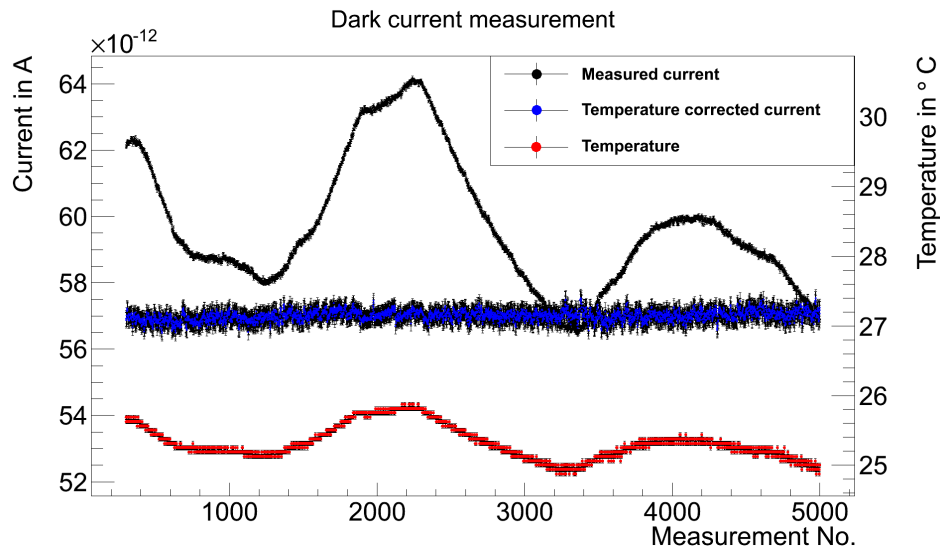
Dark current measurement

Figure 3.9: Dark current measured at the PIN diode. Each point of measurement consists of 400 readings. The black points describe the mean current (estimated as in fig. 3.8) of the single measurements. The red points show the temperature profile during the measurements. The blue points describe the temperature corrected PIN current according to eqn. 3.1.
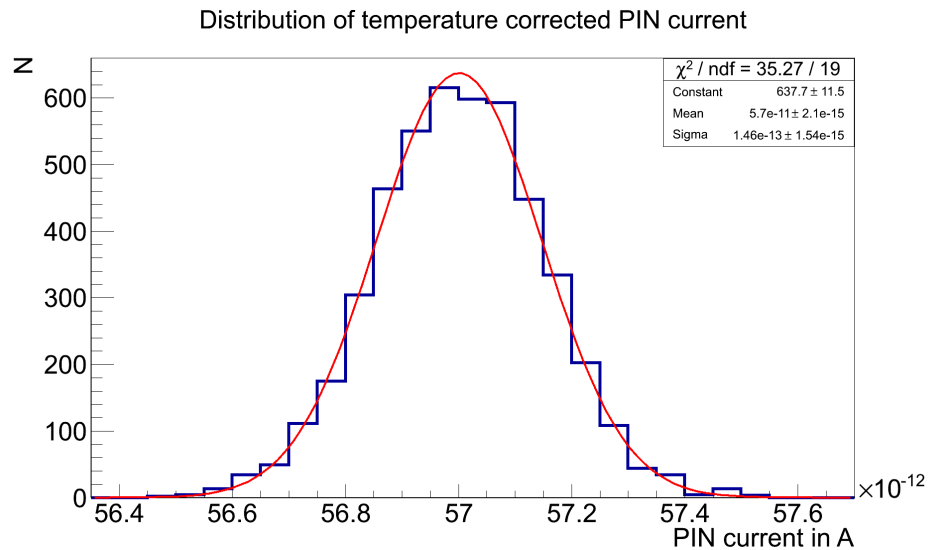
Distribution of temperature corrected PIN current

Figure 3.10: Distribution of the temperature corrected PIN current for $c_T = 0.14$ and $n_{\text{offset}} = 38$ ($\sim 30\,\text{min}$) as plotted in fig. 3.9. The fit shows that the distribution of the measured PIN currents again is gaussian.
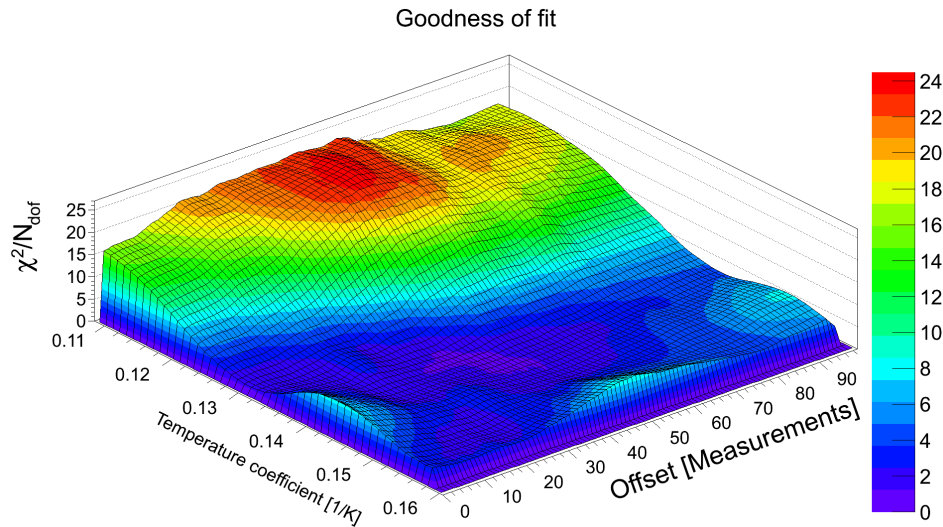
Figure 3.11: χ^2/N_{dof} of the fitted gaussian function for different sets of temperature coefficient c_T and the temperature offset n_{offset}. The parameters are chosen to $c_T = 0.14$ and $n_{\mathrm{offset}} = 38$.

Summing it all up, the long-term dark current measurement shows that the current - and thus the photon flux incident to the detectors surface - can be measured with very high precision. A measurement with 400 readings reaches a precision of 0.06%. For measurements in the range of just a few minutes - like a cycle of light and dark current measurement with each 500 readings - the temperature shift is small, and thus does not represent a problem. This is because of the fact that the temperature only affects the reverse current. The current caused by light-induced electron-hole pairs, which are proportional to the light flux, does not underlie this strong temperature dependence.

For longer measurements (of several 10 min) however temperature drift can be a huge problem. Here, the reverse current of the dark current measurement can be significantly different from the one of the actual measurement. There are two ways to handle this problem for long measurements. First, one might stabilize the temperature of the PIN diode. This could be managed with a peltier cooling. Second, the other option is to do the temperature correction as described in eqn. 3.1. The disadvantage here is that the temperature correction lowers the accuracy of the measurement. The error on the temperature corrected current ($\pm 0.42\%$) is about seven times bigger than the error on the current measurement itself (0.06%). This is due to the exponential temperature dependence of the reverse current. The error on the temperature measurement enters exponentially in the error of the current measurement.

4 Multipurpose Light Source

The multipurpose light source is an easy to use tool for different kinds of optical characterizations. With its option to provide short light pulses as well as a constant light flux it is perfectly suitable for SiPM pde measurements. But there are more possible applications, such as for example the characterization of optical fibres.

The multipurpose light source contains different kinds of LEDs to provide light over a huge spectral range from deep UV to red. The different types of LEDs and their spectra are described in chapter. 4.2. For the short light pulses different types of pulsers were tested and improved. The concept of the final version is shown in chapter. 2.3.1, the part for the constant light flux is described in chapter. 2.3.2, and the concept of the modular design of the multipurpose light source can be seen in chapter. 4.1.

4.1 Design

The multipurpose light source has a modular concept. It contains pulser-modules for short light pulses and DC modules for constant light flux (both shown in fig. 4.1). Each module contains exactly one LED and in case of the pulser module also the pulser electronics. The mainboard of the multipurpose light source has the function of providing all operating voltages and the trigger signal for the modules. It has 32 slots which all can be used for pulser and DC modules. This concept makes it easy to change or extend the light source to further wavelength ranges.

Figure 4.1: Modules as used in the multipurpose light source: Top and bottom side of the pulser module on the left and DC module on the right.

4.1.1 Pulser

The circuit of the pulser used in the multipurpose light source was developed by Franz-Peter Zantis, the head of the electronics workshop of our institute. It is a very fast pulser which is able to support pulses up to $130\,\mathrm{V}$. It is supplied with a high voltage V_{pulse} which is responsible for the high current through the LED and the supply voltages for the used operational amplifiers ($+5\,\mathrm{V}$ and $+12\,\mathrm{V}$). The high voltage pulser is triggered with a transistor-transistor logic (TTL) pulse which is a rectangular pulse of $5\,\mathrm{V}$ with a length of, in this case, $50\,\mu\mathrm{s}$.

A simplified scheme of the operating mode of the pulser can be seen in fig. 4.2. The core of the pulser is a very fast transistor. When triggered it closes the LED's circuit. The capacitor C_{pulse} is connected parallel to the voltage source V_{pulse} and placed very close to the LED-transistor circuit. Thus it delivers the energy for the pulse. In order to get a very short light-pulse it is crucial to give an extremely short trigger-pulse to the gate of this transistor. Here the parasitic gate capacitance of the transistor sets the limit on the pulse width. If the gate capacitance is sufficiently charged the transistor is activated and the LED is turned on. In order to turn off the LED the charge again has to be 'pulled away' from the gate capacitance. This means that the trigger pulse has to be not only short but also powerful. For this reason a two stage amplifier is used which decreases the time needed for the charging/discharge of the gate capacitance.

The amplifier, however, does not change the length of the incoming trigger pulse. This in turn is done by a comparator circuit. The incoming trigger pulse is led to the two stage amplifier which then opens the transistor, and to the comparator circuit at the same time. The comparator circuit delays the incoming trigger pulse by a few ns and then leads it to the other entry of the amplifier. Here it inverts the amplification direction of the amplifier and consequently the transistor is closed.

The delay of the trigger pulse happens in the following way: The incoming trigger pulse charges a little capacitor, here the pulse is delayed. The charging voltage of this capacitor is compared with a given voltage U_{width} which eventually determines the width of the light pulse. When the charge voltage of the capacitor becomes bigger than U_{width} the comparator opens and consequently changes the amplification direction of the amplifier.

The pulse width voltages U_{width}, and thus the length of the pulse, is adjusted via a trimmer which controls the relation of a voltage divider. It is manually adjusted for each pulser. Therefore the pulse is measured with an oscilloscope. The probe is attached to the source of the transistor and thus measures the source-drain voltage drop. As visible in fig. 4.3, the voltage drops from the high voltage (here $70\,\mathrm{V}$) to zero in $\sim 2\,\mathrm{ns}$. The whole pulse takes about $7\,\mathrm{ns}$. The fact that the pulse seems to drop below zero and the oscillation behind the pulse are due to the impedance mismatch

of the probe and the circuit. This pulse width measurement is done for every pulser module to guarantee that every pulse has a length of about $7 \pm 1\,\mathrm{ns}$.

The pulse width is shorter than the shortest SiPM recovery time and the possibility of pulse voltages up to $130\,\mathrm{V}$ promises to cover a huge dynamic range. When working with a low number of photons per pulse, the maximum pulse rate of $50\,\mathrm{kHz}$ is helpful to get a good signal-to-noise ratio at the reference detector.
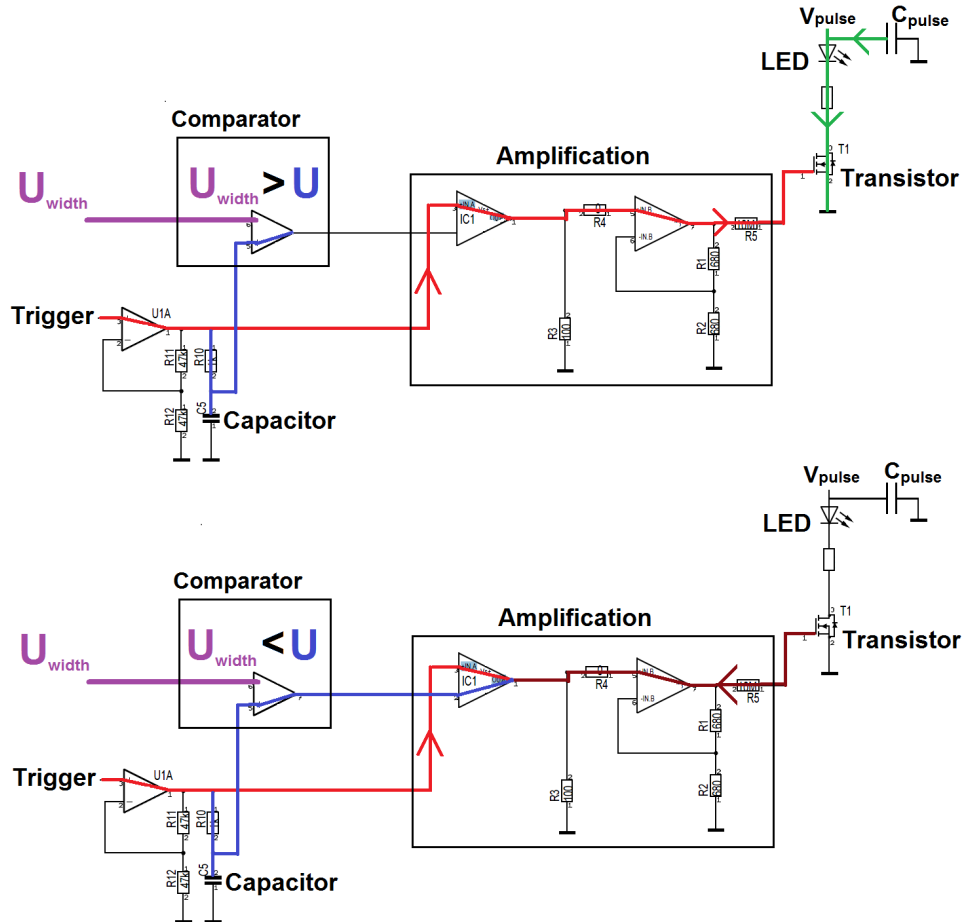

Figure 4.2: Simplified schematic of the pulser-module (developed by Franz-Peter Zantis). Top: LED is on. Bottom: LED is off.

4.1.2 DC Source

The DC module is of a rather simple structure compared to the structure of the pulser-module. It contains the electronics for the module-type detect function and connects the LED with the power supply connected to the multipurpose light source. In order to establish a constant light flux the LED has to be driven at a constant current. This is so, because the light output in first approximation is proportional to the current through the LED.
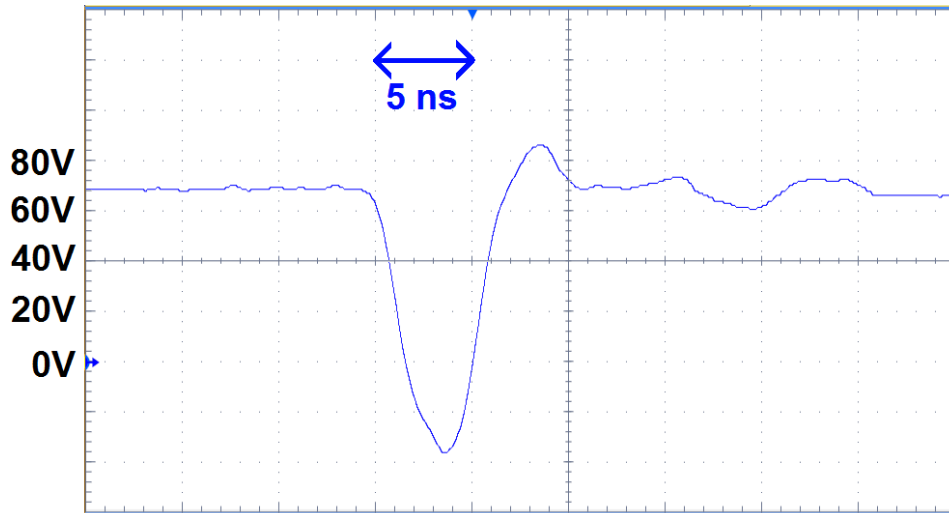
Figure 4.3: 70V pulse measured at the transistor from source to drain. The rising
        edge is about $35\,\mathrm{V/ns}$ steep. The fact that in this measurement the pulse
        peak goes below zero, is only because of the impedance mismatch caused
        by using a probe. The oscillations at the end are caused by the same
        reason.

One method is to use a current source that holds an adjusted current. Another
method is to use a voltage source in combination with a series resistor. The series
resistor reduces the current variations. The forward current through a diode rises
exponentially with the voltage. Adding a resistor lessens the voltage dependence of
the current. This method is used for the measurements in chapter. 5.4.

4.1.3 Mainboard and Housing

The heart of the mainboard is a microcontroller. It establishes the connection to a
computer from which the light source can be controlled and manages which voltages
and signal are applied to which module. Therefore it is connected to a chain of shift
registers. These shift registers switch about 100 electromechanical relays to connect
and disconnect the modules from the mainboard.
Relays are used because they perfectly disconnect the unused modules from the main-
board and have a high dielectric strength which is needed because of the high pulse
voltage, whereas transistors, especially in high voltage and current versions, always
have a certain leakage current and a rather high parasitic terminal capacitance. The
latter would possibly cause problems with the trigger pulse.
For the pulser module three different operating voltages are needed, $+5\,\mathrm{V}$ and $+12\,\mathrm{V}$
for several operational amplifiers and the pulse voltage V_{pulse} which controls the cur-
rent pulse though the LED. +12V also is the operating voltage of the mainboard.
The other two voltages are each generated by a DC/DC converter. One of them is

a special high voltage DC/DC converter which generates pulse voltages between $0\,\mathrm{V}$ and $130\,\mathrm{V}$. The output of the high voltage DC/DC converter is proportional to an adjustment voltage between $0\,\mathrm{V}$ and $5\,\mathrm{V}$. The use of a 16-bit digital to analogue converter for this adjustment voltage enables a theoretical precision of $2\,\mathrm{mV}$ for V_{pulse}. This is well below the ripple of the high voltage module given by the manufacturer (0.03% at maximum voltage). Additionally there is also the possibility of using an external voltage supply for V_{pulse}. The trigger signal for the pulser-module is not generated on the mainboard but comes from an external device which is plugged to the light source.

The current source for the DC module is not implemented in the mainboard yet. This means that an external current source has to be plugged to the light source to supply the DC modules. Nevertheless the main board is prepared for an upgrade with an internal current source.

Another useful feature of the multipurpose light source is the module type-detect function. It allows to read back whether a connected module is a pulser or a DC module. For this purpose, one of the connection pins of the module is pulled up to $+5\,\mathrm{V}$. A chain of shift registers is used for the detection of this signal. A scheme of the mainboard and the positioning of the modules is shown in fig. 4.4. As one can see, the modules are arranged so, that all LEDs are in a row. Thus a moveable stage can be positioned along the line of LEDs. This way the light of one LED is coupled into an optical fibre.
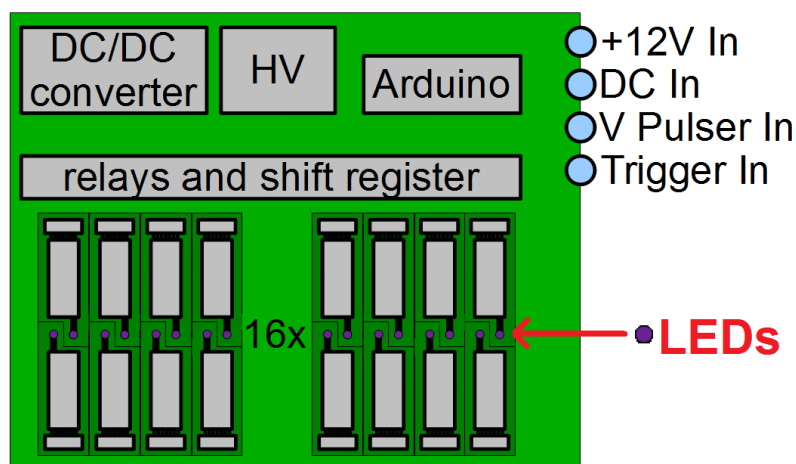

Figure 4.4: Sketch of the multipurpose light source's mainboard. It contains DC/DC converters, a microcontroller (Arduino) and a chain of shift registers which switch various relays. At the bottom one can see the two rows of each 16 DC- or pulser-modules.

The housing and the moveable stage has been designed by Carsten Heidemann. The housing is made from $5\,\mathrm{mm}$ thick aluminium panels. A picture of the multipurpose light source can be seen in fig. 4.5. At the front which is shown in fig. 4.6) it has four external inputs: +12V supply voltage (mainboard), trigger and optional high voltage (pulser module) and DC (DC module). Further there are two air outlets for the airstream created by the two fans at the backside (see fig. 4.7).

The pulser- and DC modules are mounted to the bottom of the light source's top. This way the LEDs are visible through the holes in the top. This and the mechanism for the light pick up can be seen in fig. 4.8. The moveable stage runs on a threaded rod which is moved by a stepper motor. Once the optical fibre is positioned over the LED the mechanism shown in fig. 4.8 lowers the fibre directly on top of the LED.

4.2 LEDs

The light emitting devices of the multipurpose light source are LEDs. An LED (light emitting diode) is a semiconductor and it has the typical electrical properties of a diode. The difference to other diodes is that the used pn-junction material has a direct band gap instead of an indirect. This means no crystal momentum transfer is necessary during recombination. As a result the emission of a photon is much more probable [20]. The photon wavelength is determined by the energy difference of the valence and conductive band.

The forward current through a diode, in this case a light emitting diode, is given by the Shockley equation:

$$I_D = I_S(T)(e^{\frac{U_F}{nU_T}} - 1) \tag{4.1}$$

Here U_F is the voltage across the diode and U_T is the thermal voltage which is about $26\,\mathrm{mV}$ at room temperature. $I_S(T)$ is the saturation current and n is the ideality factor and normally has a value between one and two. At operation voltage the current rises exponentially with the voltage, this means that small variations of the voltage cause significant changes of the current. The intensity of the emitted light mainly depends on the forward current I_D because every electron passing the pn-junction has the ability to emit a photon. Another factor that affects the light intensity is the junction temperature. As a result the functional connection between light intensity and current can be different for various LEDs.

For the multipurpose light source different types of light emitting diodes are used which are listed in table 4.2. A set of special UV LEDs covers the spectrum from $320\,\mathrm{nm}$ to $400\,\mathrm{nm}$. Further LEDs cover the spectrum up to $650\,\mathrm{nm}$. Some of them

are high-power LEDs which can be driven at currents up to 1.5 A. Among them is a white light LED which has a spectrum ranging from 450 nm to 650 nm. The white light LED is the only one which is not possible to pulse. This is due to its operation mode. A blue LED excites phosphor molecules which emit a spectrum of photons with lower energies, and so accordingly a white light spectrum is emitted. The pulse width is downwards limited by the time constant of the phosphor luminescence - typical decay times range from $\sim 1\,\mu s$ to a a few seconds - which is much longer than the required pulse width.

The spectra of the LEDs used for the light source were measured with an 'ocean optics USB650-UV-VIS' spectrometer [28]. It has a grating to fan out the incoming light and a Sony ILX511 linear silicon CCD array detector with 2048 pixels to measure the spectrum from $200 - 850\,$nm. The optical resolution of the spectrometer is $\sim 2\,$nm. The measured spectra of the LEDs used for the pulser and DC modules can be seen in fig. 4.9 and 4.10. Plotted on the Y-axis is the number of counts of the corresponding CCD pixel. At 600 nm one count corresponds to 41 photons.

Due to the modular set up of the light source and the vast variety of available LEDs, the spectrum is easily extendable with nearly every wavelength from the deep UV range to infrared.

LEDs are perfectly suited for short light pulses as well as for constant light flux. This together with their long life time makes them the best choice for the multipurpose light source.

4.3 Operation of the Multipurpose Lightsource

This chapter will give a short introduction on how to control the multipurpose light source via USB from a computer. There is a C-program on the light source's Arduino which receives commands via USB and then operates the multipurpose light source accordingly. A list of the most common commands is found in fig. 4.1. Once the connection to the light source is established (for example with the 'Arduino serial monitor' or a LINUX terminal) a list of all available Arduino commands can be shown with `help`. The command `LED x` activates LED No. x. A list with all LEDs, their type designation, module-type, wavelength and typical current is shown in table 4.2. With `SwitchHV x` the high voltage source for the pulser can be switched: x=0 means external and x=1 means internal. The high voltage itself is changed by `HV x`. This value has to be between 0 and 130. Anything else will be ignored. Finally one of the two optical fibres has to be moved above the chosen LED. Here `move1 x` moves the right fibre above LED No.x and `move2 x` the left fibre.

In order to get a fully automated measurement these commands are implemented in a program which also manages the settings for external devices which are plugged to

the light source. The sourcemeter which measures the photocurrent of the reference detector is also controlled by this program.

All in all one can say that the multipurpose light source is an important milestone on the way to a fully automated SiPM teststand. It has two light-outputs which both can provide short light pulses and a constant light flux over a broad spectrum. All adjustments for the light source and its surrounding devices are completely computer controlled and therefore this means that test sequences can be planned in advance and executed fully automated.

Command	Function
help	Displays the help
LED X	Turns on LED X
SwitchHV X	Switches HV supply. extern X=0, intern X=1
SwitchTrigger X	Switches Trigger. extern X=0, intern X=1
SwitchDC X	Switches DC supply. extern X=0, intern X=1
HV X	Set HV(intern) to X volt
off	Switches all supplies to extern and all LEDs off
move1 X	Moves the right fibre to LED no.X
move2 X	Moves the left fibre to LED no.X

Table 4.1: List of installed LEDs

LED No.	LED-type	Module-type	λ_{peak} in nm	I_{typ} in mA
1	LUMITRONIX 15401	Pulser	399	100
2	LUMITRONIX 15401	DC	399	30
3	XSL-355-5E	Pulser	352	100
4	XSL-355-5E	DC	352	25
5	TLCY5800	Pulser	591	1000
6	TLCY5800	DC	591	50
7	HLMP3519	Pulser	558	500
8	HLMP3519	DC	558	25
9	HLMP-CB14	Pulser	463	100
10	HLMP-CB14	DC	463	30
11	UVTOP315-BL-TO18	Pulser	315	200
12	HLMP-CE14	DC	506	30
13	TLHB580	DC	410-470	30
14	TLDR580	DC	650	30
15	HLMP-CE14	Pulser	506	100
16	UVTOP335-BL-TO18	Pulser	335	200
18	CreeXP-E rot-orange	DC	621	1000
19	CreeXP-G Q2	DC	470-700	1500
20	NSPG500DS	DC	526	35
21	NSPY500DS	DC	510-650	35

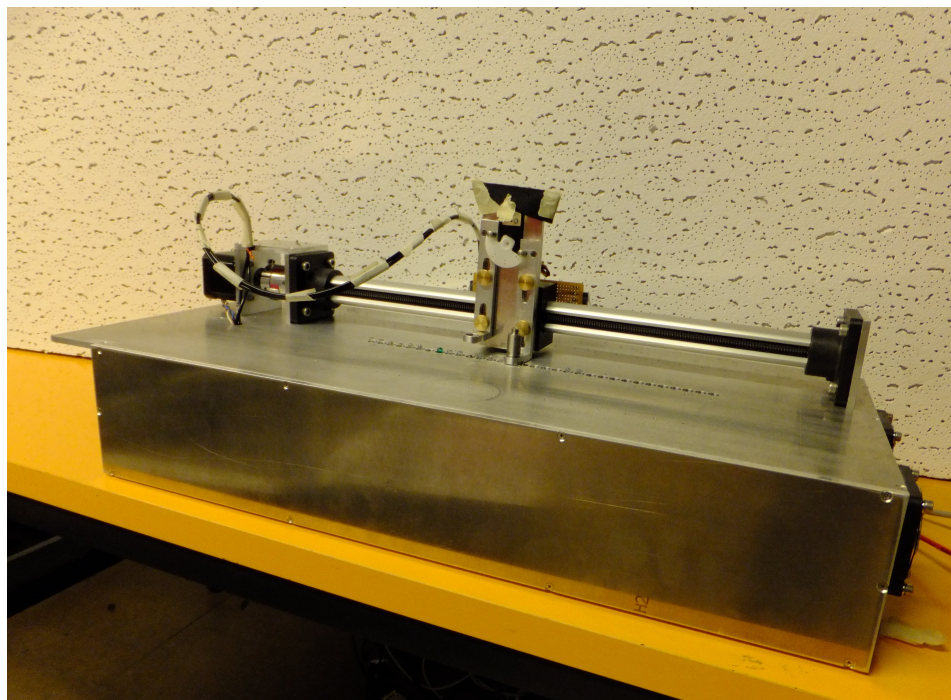Table 4.2: List of installed LEDs

Figure 4.5: The multipurpose light source

Figure 4.6: Front of the multipurpose light source. At the top there are 3 connectors for the external voltages. At the bottom there are a USB-connector and a lemo-connector for the trigger signal.

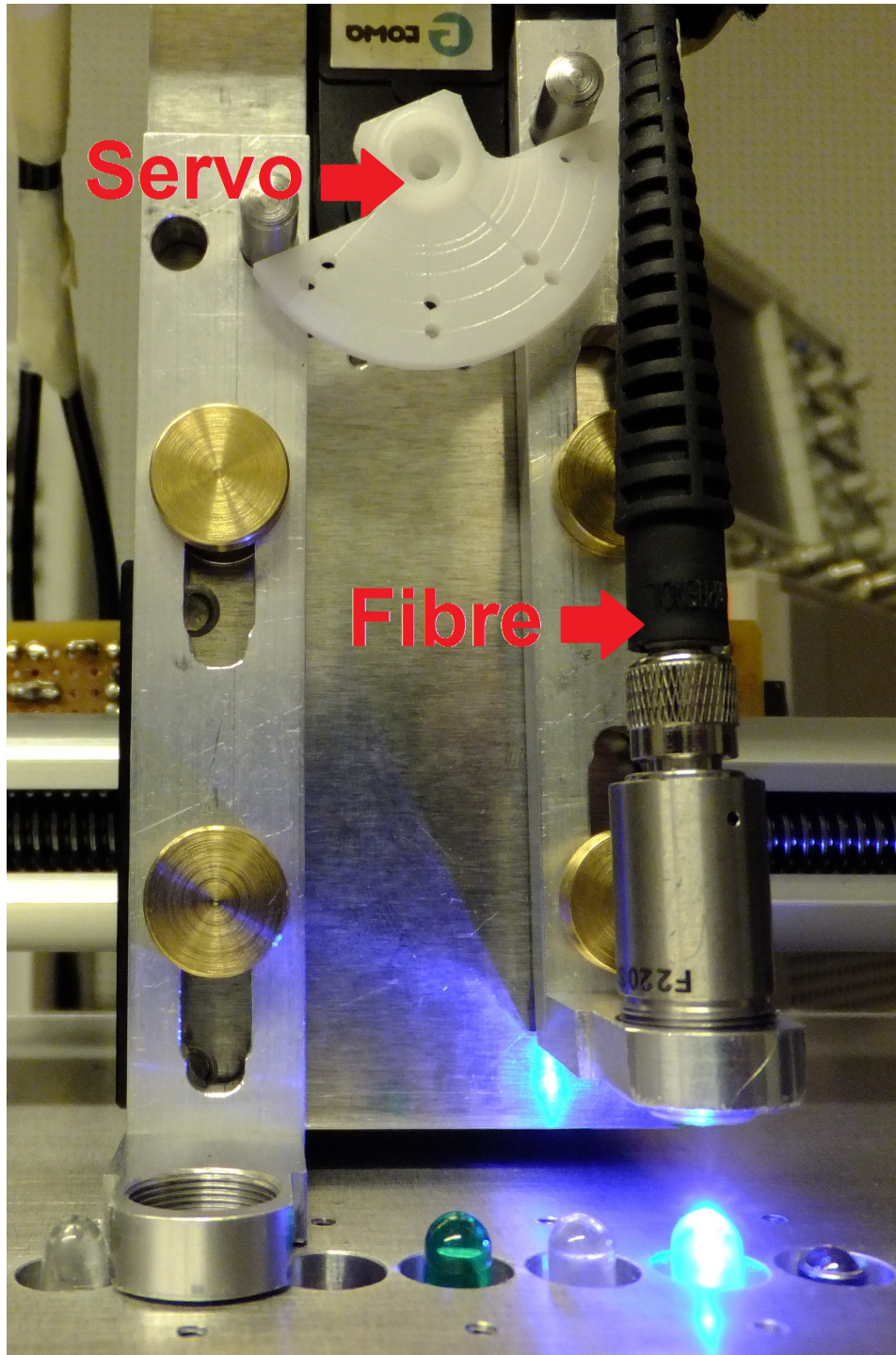Figure 4.7: Back of the multipurpose light source with the two fans.

Figure 4.8: The movable stage of the multipurpose light source. The white wheel is moved by a servo. Thus the two arms with the optical fibres can be moved up and down. In the picture the right arm with collimator and optical fibre is in the up-position. It can be lowered directly on top of the blue LED.
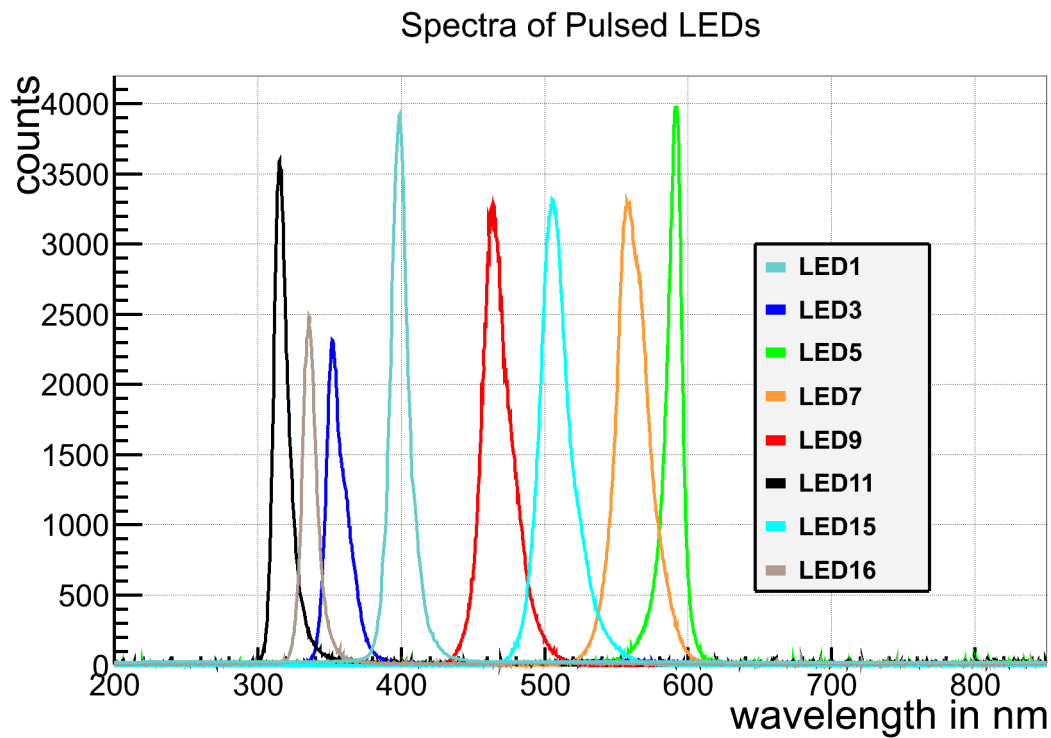
Figure 4.9: Spectra of the LEDs of the pulser-modules. There is no correlation between the counts and the absolute maximum intensity of a LED.
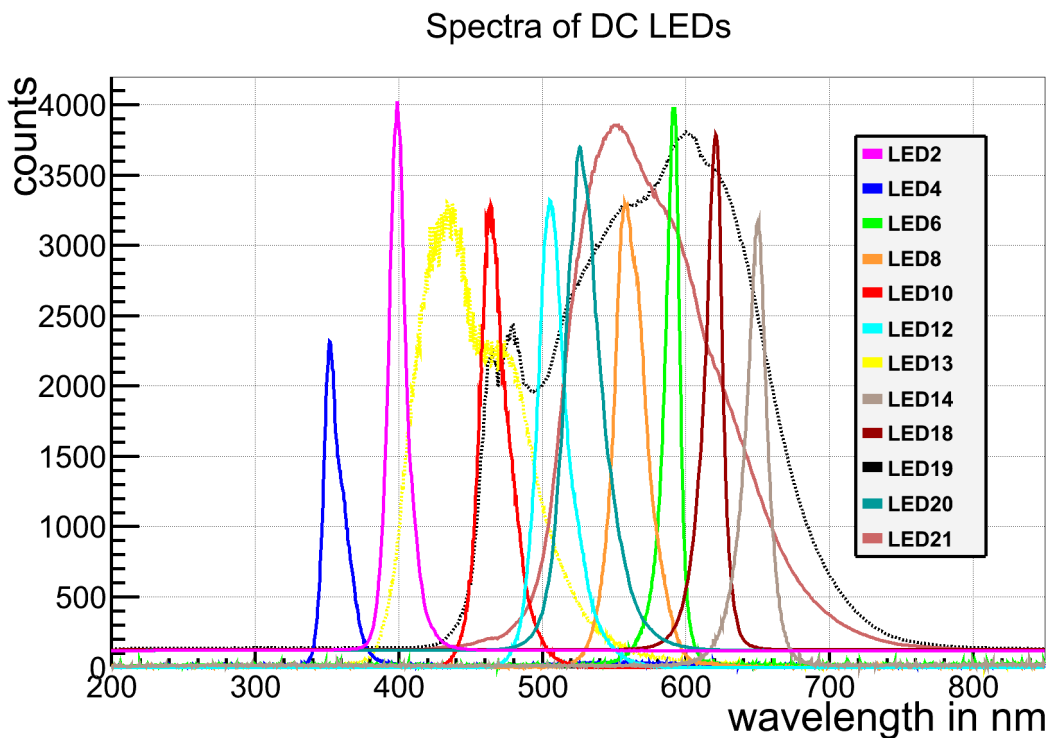
Figure 4.10: Spectra of the LEDs of the DC modules. There is no correlation between the counts and the absolute maximum intensity of a LED.

5 Performance

In this chapter the performance of the multipurpose light source is presented. Therefore several measurements are done with pulsed and constant light. These measurements are not meant as a calibration of the multipurpose light source. In fact, there is no precise calibration needed. The concept is not to adjust certain parameters which yield a fixed light output, but to vary the parameters until the desired light flux is established. This is because there are to many factors like temperature, change of the optical fibres' bending, and position of the collimator above the LED that change the quantity of light that is incident to the detectors surface.

The dynamic range and the accuracy of the light source is demonstrated on the basis of four LEDs. These LEDs are chosen to cover a wavelength range of our interest. The tested LEDs are a deep UV-LED, a UV-LED, a blue LED, and a green LED. Except for the spectral transmission measurement for all measurements the reference detector (PIN diode) was used. It's measured quantity is the photocurrent from which one can derive the number of incident photons per second which is

$$\#\gamma/s = \frac{I_{\text{photo}}}{e \cdot \text{q.e.}(\lambda)}. \tag{5.1}$$

Due to the wavelength dependence of the PIN diode's quantum efficiency this quantity not only depends on the photocurrent but on the wavelength, too. The number of incident photons per measured photocurrent will be useful for some rough calculations in the following chapters and thus is derived for all LED's wavelengths. It can be found in table 5.1. For the derived values only the quantum efficiency of the LED's peak wavelength was used. For more precise measurements it would be better to integrate the quantum efficiency over the LED's spectrum.

LED No.	LED-type	λ_{peak} in nm	$\#\gamma/s$ at $1\,\text{pA}$
1 and 2	LUMITRONIX 15401 (blue)	399	$7.8 \cdot 10^6$
3 and 4	XSL-355-5E (UV)	352	$11.4 \cdot 10^6$
15 and 12	HLMP-CE14 (green)	506	$7.1 \cdot 10^6$
11	UVTOP315-BL-TO18	315	$17.8 \cdot 10^6$

Table 5.1: The set of LEDs used for the measurements in this chapter
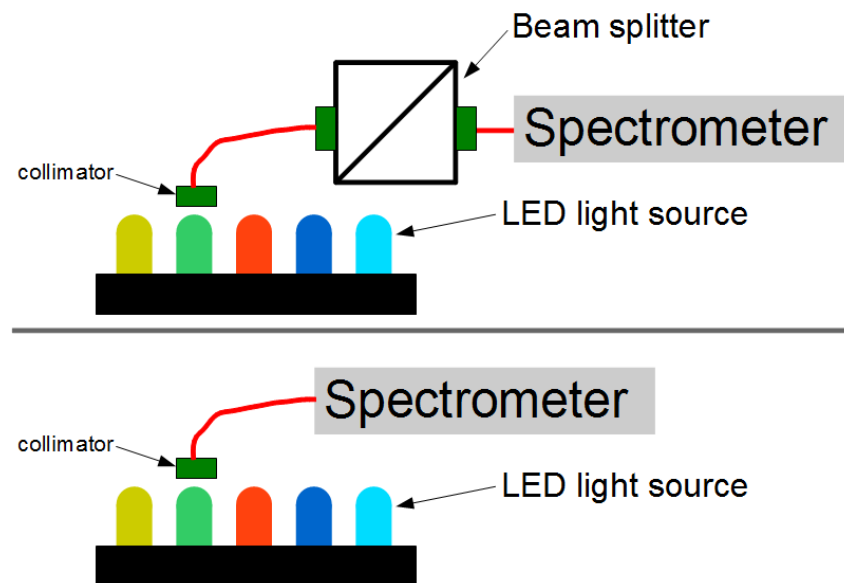
5.1 Spectral Transmission Measurements

Figure 5.1: Scheme of the two set-ups for the transmission measurement.

The optical path between light source and reference detector is, especially in the UV range, absorbing a huge amount of light. Most light is absorbed in the beam splitter, but also the two collimators with the attached optical fibres at its input and output have a measurable effect. In order to determine the transmission of the optical path the multipurpose light source and the spectrometer (see chapter 4.2) are used. The spectrometer and the characterized optical components are part of the SiPM test-stand (see chapter. 2.1).

The transmission is the ratio of two measurements with different set-ups: For the first set-up the light source is directly connected to the spectrometer, for the second set-up the beam splitter in transmission direction, the two collimators (one at the input and one at the output of the beam splitter) and an additional optical fibre are put in the line between light source and spectrometer. A scheme of both set-ups can be seen in fig. 5.1 It is useful to do the measurements in this order (measurement with higher signal first) to be able to adjust the light source so that the dynamic range of the spectrometer is fully used. The measurements are done with two different blue LEDs, a UV, and a white light LED (LED No. 2, 4, 10, and 12). The result of the measurements can be seen in fig. 5.2. The unit 'counts' on the y-axis refers to the weighted number of counts of the CCD pixel and is a measure for the intensity at this wavelength. As there are no further specifications about the weighting the error is supposed to be poissonian. The four plots in fig. 5.2 show the measurements with the four different LEDs. For the regions where the lower measurement has at least 125 counts the transmission is derived. The combined results of all measurements

can be seen in fig. 5.3. The spikes at the ends of the different measurement ranges appear because of the small signal to noise ratio in these regions. The pink circles depict the transmission of the beam splitter (as read off from fig. 2.2) minus the reflections at the collimators' surfaces which is each time 4.2%. The reflection at the collimator surface is derived from the refraction index of the collimator glass (D-K59) at 587.6 nm under the simplification of perpendicular light incidence (transmission values by the manufacturer are not given). The loss due to the optical fibre is 1% at 350 nm and negligible for higher wavelengths (see fig 2.3). Reasons for the discrepancy of measured and calculated data can be: The wavelength dependency of the reflection at the surfaces of the collimators, the wavelength-dependent focal shift of the collimators, remaining divergence of the collimated light travelling through the beam splitter and thus losses at the second collimator when coupling the light into the fibre again, and a lower transmission in the UV range.

5.2 Set-up and Method of Measurement

The set-up used for the performance measurement is part of the SiPM teststand which is presented in chapter. 2. The used light path - in short - consists of: LED - collimator - optical fibre - collimator - two beam splitters - collimator - optical fibre - diffuser - PIN diode (for more details see chapter. 2.1). The photo current is measured with a sourcemeter (Keithley 2614b) which also supplies the PIN diode with a bias voltage of 10 V. Each measurement consists of 500 readings which are filled into a histogram. The mean of a gaussian function fitted to this measurement is the measured current value. An example measurement can be seen in fig 5.4. Although the readings are gaussianly distributed, the error of this measurement is not, as one might expect, the sigma of the estimated gaussian function divided by the number of readings. There is at least one other error which is not of statistical nature. One possibility is that variations in the mains frequency are responsible for this error. The measurement time is given in units of power line cycles. If the real mains frequency differs from 50 Hz this can lead to deviations in the measured value (because the sourcemeter does not measure and adjust to the real mains frequency). There are to ways this can affect the measurement: If the sourcemeter's integration time does not match exactly one power line cycle the strength of the coupling of noise signals depends on the phase at which the integration starts. Second, the strength of the noise signal itself can depend on the mains frequency.
However, the sourcemeter accuracy of 0.06% for a dark current corrected measurement [23] given by the manufacturer seems to be a more reasonable value for the error than the sigma of the gaussian function.
In order to remove the PIN diode's noise from the measurement a dark current meas-

urement is done directly after each measurement. This dark current measurement is subtracted from the light measurement.
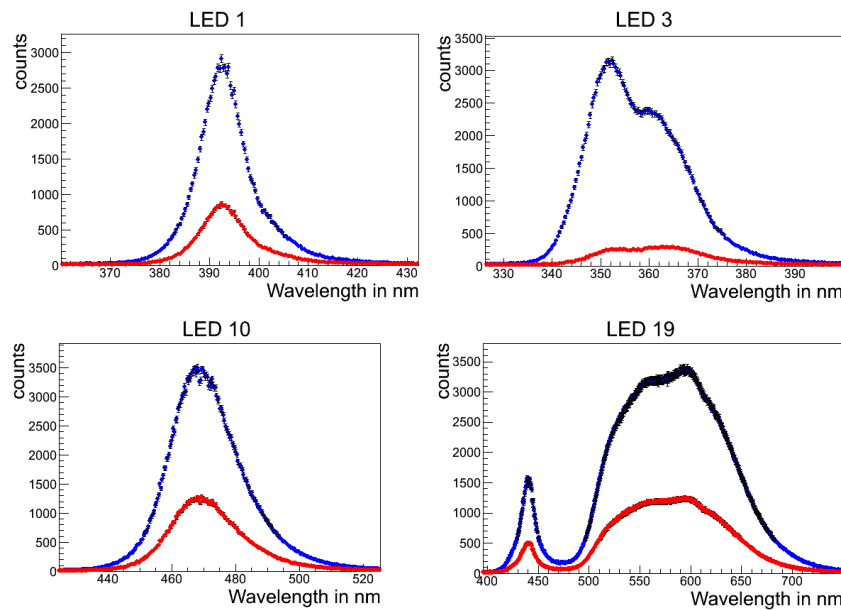

Figure 5.2: Results of the transmission measurement. The plots each show the measurement without beam splitter in blue and the measurement with beam splitter in red. The transmission of the beam splitter (plus fibre and collimators) is the ratio of these two measurements.

5.3 Pulser-Module Performance Measurements

In order to demonstrate the accuracy and reproducibility of the multipurpose light source's pulse mode several measurements with the same set-up are done. For this measurement it is important to achieve a constant light output over several measurements. This means that the thermal properties of the LED become important. There are mainly two effects that influence the LED's light output with changing junction-temperature. On the one hand the current increases with rising junction-temperature. On the other hand the efficiency of the light emission decreases with rising junction temperature [20]. According to whether the one or the other effect predominates the light output increases or decreases with the temperature.

This means that the LED has to heat up before the measurement is done. The time until thermal equilibrium is reached varies for the different LEDs. In order to get an idea of the order of magnitude of this time a series of successive measurements is done. In fig. 5.5 one can see that throughout these measurements the LED's light output stabilises. Due to the very small duty cycle of 0.007% at the pulse frequency of 10 kHz the junction temperature is not only determined by the forward current
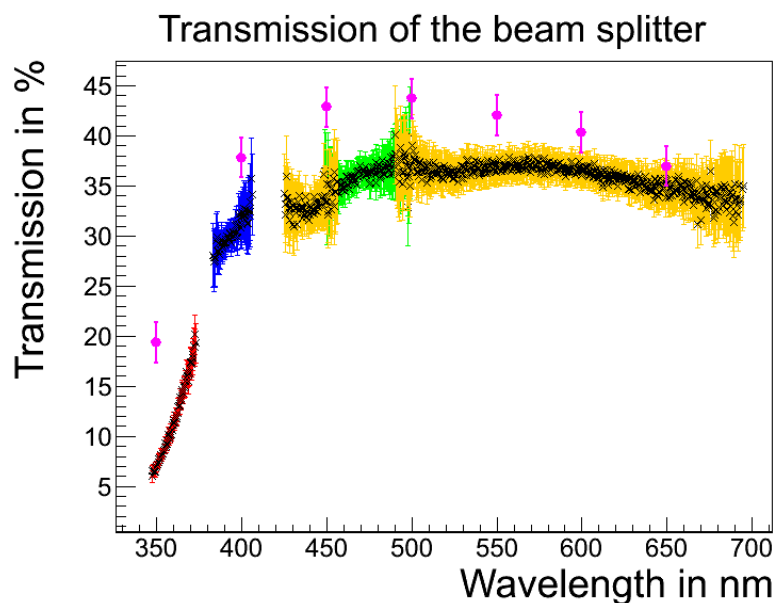
Figure 5.3: Transmission of the beam splitter (plus fibre and collimators) as derived from the measurements. The different colours indicate the spectral range of the different used LEDs (Red=LED3, blue=LED1, yellow=LED19, and green=LED10). The pink circles show the combined transmission as taken from the data sheets of the beam splitter, optical fibre and collimators

but as well by the ambient temperature. This might explain the variations in the last 25 minutes of the measurement series.

As a result from this the LED is already pulsed ten minutes before every single light measurement in order to reach thermal equilibrium. Directly after the light measurement the dark current is measured. A dark current measurement directly before the light measurement is not possible because of the fact that the LED is switched on 10 minutes before the light measurement. As interfering signals change with time the dark current measurement is supposed to be as close as possible to the light measurement. For this reason a dark current measurement before the light measurement is not taken into account.

The difference of these two measurements (dark current and light measurement) is the photocurrent caused by the light source and the error on the photocurrent is 0.06% of the uncorrected light measurement. Fig. 5.6 presents 25 of this photocurrent measurements taken during five hours. The fit of a constant to these data shows that within the errors the light source produces reproducible light pulses. From the mean photocurrent of these measurements one can derive the number of photons per pulse and area. Using table 5.1 and recalling that the sensitive area of the reference detector is $25\,\mathrm{mm}^2$ leads after a rough calculation to about 12 ± 2 photons per pulse and mm^2 for the data presented here. This is close to the aim of one photon per pulse
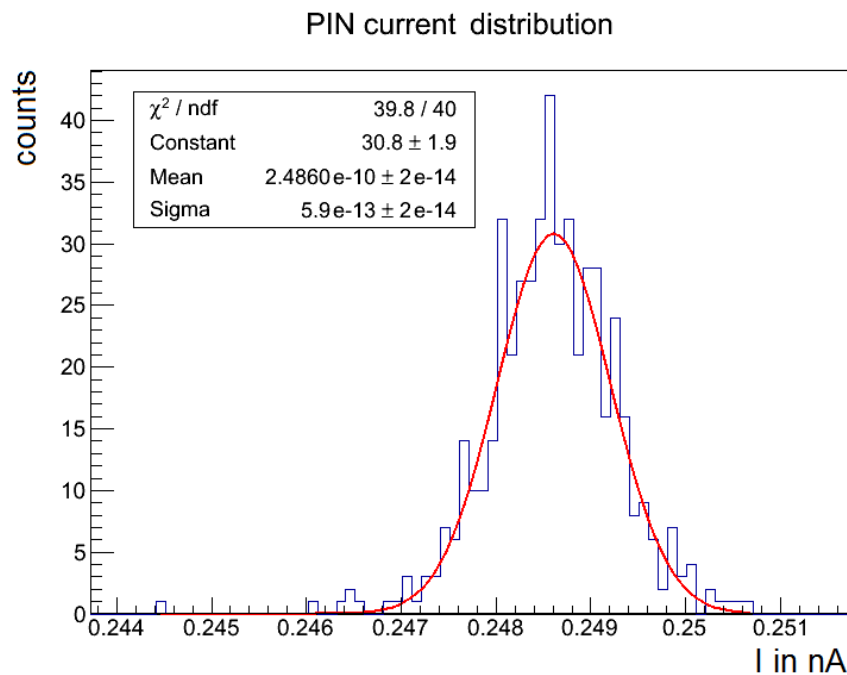
PIN current distribution

Figure 5.4: Histogram of the 500 readings of one measurement (LED 15 at 50 V and 20 kHz). The mean of the fitted gaussian function is the measured current value.

and mm^2. The same measurement for LED 3 and LED 15 can be seen in fig. 5.7 and fig. 5.8.

A similar measurement is done with the deep UV LED 11 which has a peak wavelength of 315 nm. At this wavelength the beam splitter has a negligible transmission and thus is removed from the test set-up for this measurement. The results of the measurement in fig. 5.9 demonstrate that the pulser module is able to create pulses with just a very few photons. The average photocurrent of the shown measurements corresponds to a number of 5 ± 1 photons per pulse and mm^2.

Further properties of interest are the frequency and voltage dependency of the light output. The figures in 5.10 show measurements of the photocurrent at different pulse repetition frequencies. The photocurrent behaves exactly as expected, in first approximation it rises proportionately with the pulse repetition frequency.

In order to investigate the voltage dependence and the dynamic range measurements at different voltages are done. The measurements are shown in the fig. 5.11 and fig. 5.12. The measurements show that the photocurrent rises more or less linear with the pulse voltage; but there is no obvious functional correlation between measured photocurrent and pulse voltage. The measurement series for LED 1 was done twice. The difference between these two measurement series is about 20%. This
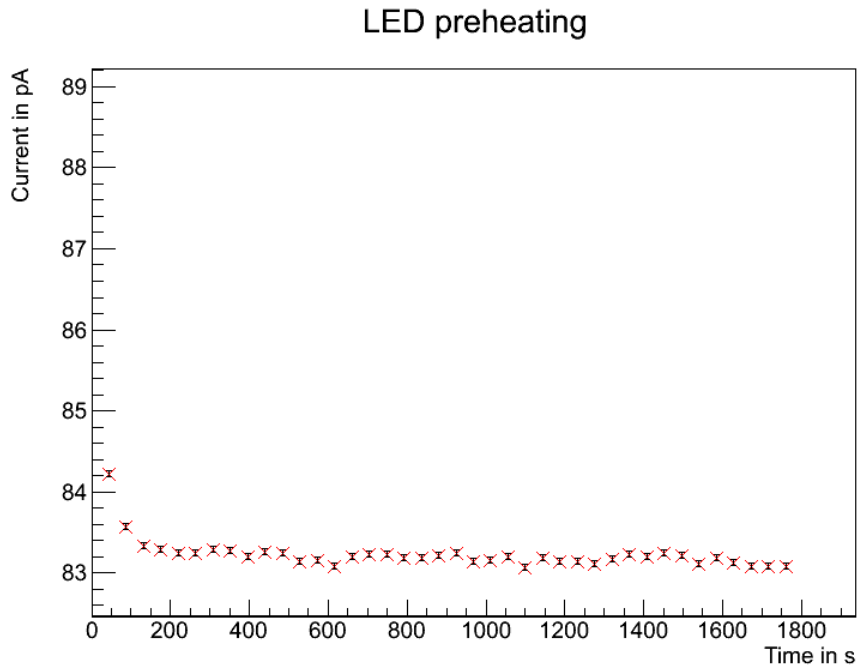
Figure 5.5: Measured photocurrent of LED1 while heating up. $V_{pulse} = 10\,\text{V}$ and $f = 10\,\text{kHz}$

huge difference is because of the mechanical connection of the light pick-up and the collimator. The collimator can move in the light pick-up and thus has a different orientation when the slide was moved, and thus gathers a different amount of light. This problem will be solved soon as a new holder is already built and just has to be installed. This means that the performance of the light source as presented still has potential to be improved by this update. However, in order to check if the pulse voltage supply works as expected this measurement series should be done again with the new holder.

Another interesting information that can be derived from these measurements is the upper limit of the pulser module's dynamic range. A rough calculation of the number of photons per pulse and mm^2 leads to numbers of over 1800 for LED 1 and over 4100 LED 15, and at least 200 for LED 3 (Here most of the UV-light is absorbed in the beam splitters). These values for the visible light emitting LEDs 1 and 15 are high enough to drive most of the available SiPM into saturation, although the pulser is not even used at its limit of 130 V. The low number of photons per pulse for LED 3 is because of the bad UV transmission of the two used beam splitters.

5.4 DC Module Performance Measurements

The three tested DC modules have the same LED types as the pulser modules in the previous chapter. The current source used for the measurements is the same as presented in chapter. 4.1.2: A voltage source with current limitation in combination with a series resistor of $300\,\Omega$. The method for the photocurrent measurement stays the same as for the pulser module measurements. The only difference is that because of the huge expected signal-to-noise ratio no dark current measurements are done. The results of three exemplary measurements are shown in fig. 5.13, fig. 5.14 and fig. 5.15. As one can see, there are some variations in the photocurrent which occur mainly because of two reasons. First, the heating-up of the LED changes its efficiency which causes variations at a long time scale. After a certain time the variation based on the heating-up stagnates. Second, the regulation fluctuations of the voltage source lead to a noise-like variation on a short time scale.

After a preheat time of approximately one hour the second effect is dominating. Then the peak to peak fluctuations are smaller than 0.8% for all three modules. In order to interpret this fluctuation one has to recall that within the SiPM teststand the DC module is used for relative pde measurements (for more details see chapter. 2.2). Here the SiPM's current signal is directly compared to the reference detector's photocurrent. Consequently, fluctuations as measured for the DC module are not expected to have big influence on the relative pde measurement.

Another important property to look at is the light intensity and the rate of emitted photons respectively. Some rough calculations will show that the light intensity is in the right order of magnitude for the planned measurements. For the light emitted by LED 2 the quantum efficiency of the reference detector with its $25\,\mathrm{mm}^2$ sensitive area is about 80% (see fig. 3.3). This means that a current of $43\,\mathrm{nA}$ corresponds to a photon flux of approximately $13\ \mathrm{mm}^{-2}\mathrm{ns}^{-1}$. For a typical SiPM the recovery time is around $10\,\mathrm{ns}$. As a result one can say that the DC module definitely is powerful enough to trigger enough SiPM cells to achieve a good signal-to-noise ratio. A higher photon flux is not desired because of the rising number of double hits. With more double hits the measurement becomes less sensitive for the SiPM's pde. The photon flux for LED 4 which is in the UV range with approximately $0.2\ \mathrm{mm}^{-2}\mathrm{ns}^{-1}$ is lower than for the others. This is due to the low UV transmission of the beam splitters. Nevertheless, even with this value measurements are possible.
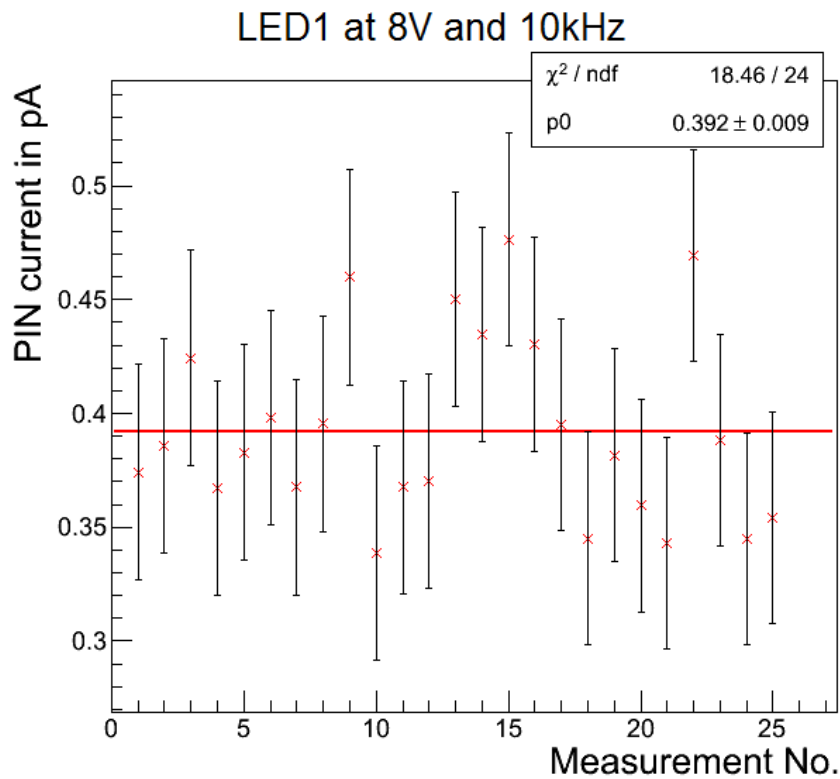
Figure 5.6: Difference of the photocurrent between measurement with light and dark measurement (for LED1 with $\lambda = 399\,\mathrm{nm}$). All measurements are compatible with the mean of $0.39\,\mathrm{pA}$
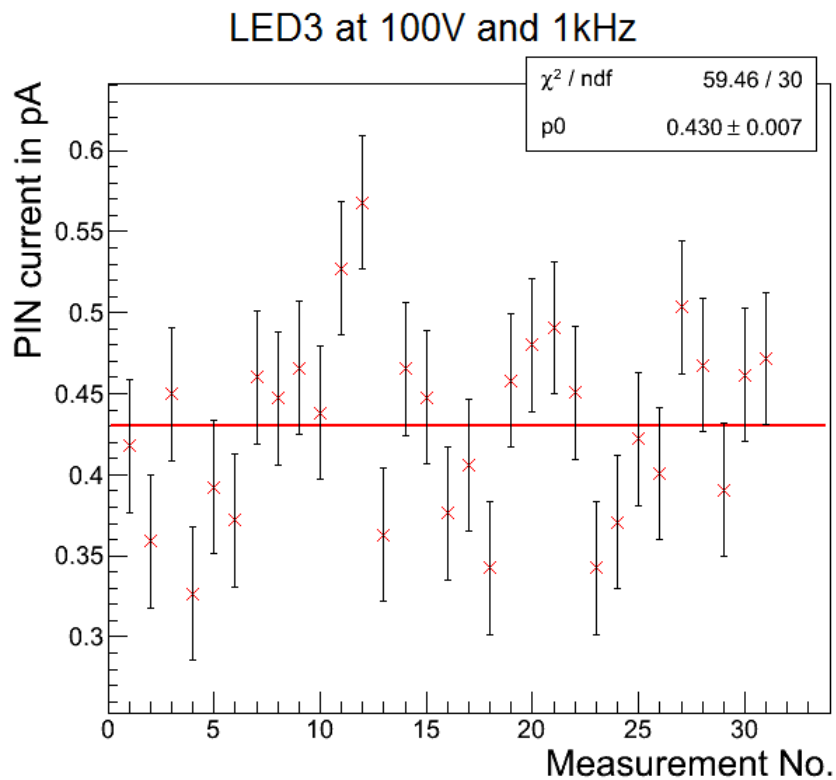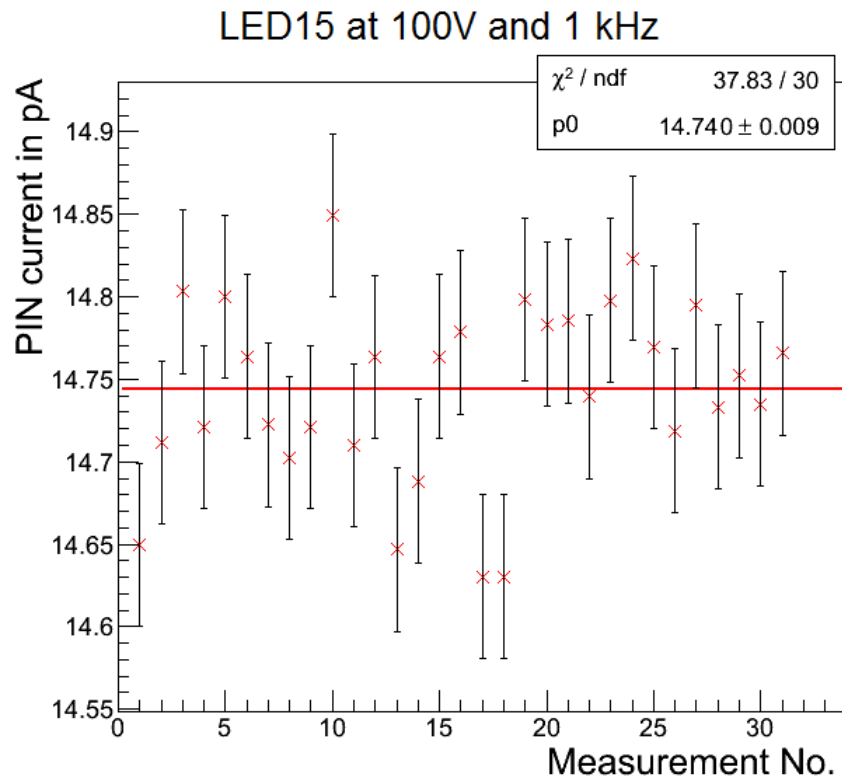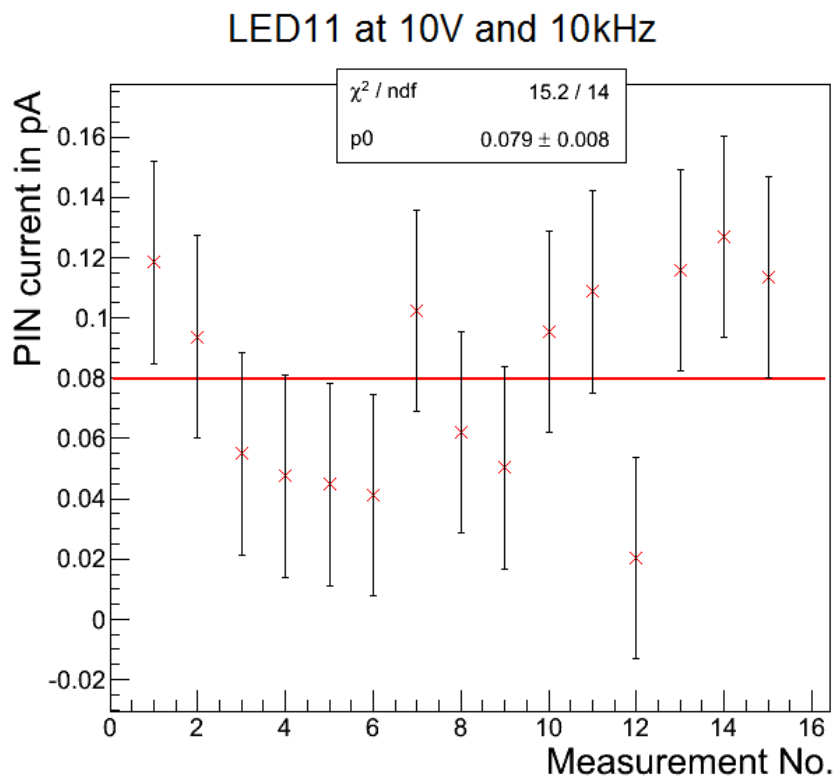

Figure 5.7: Difference of the photocurrent between measurement with light and dark measurement (for LED3 with $\lambda = 352\,\mathrm{nm}$). All measurements are compatible with the mean of $0.43\,\mathrm{pA}$

Figure 5.8: Difference of the photocurrent between measurement with light and dark measurement (for LED15 with $\lambda = 506\,\mathrm{nm}$). All measurements are compatible with the mean of $14.74\,\mathrm{pA}$

Figure 5.9: Difference of the photocurrent between measurement with light and dark measurement (for LED11 with $\lambda = 315\,\mathrm{nm}$). All measurements are compatible with the mean of $0.079\,\mathrm{pA}$
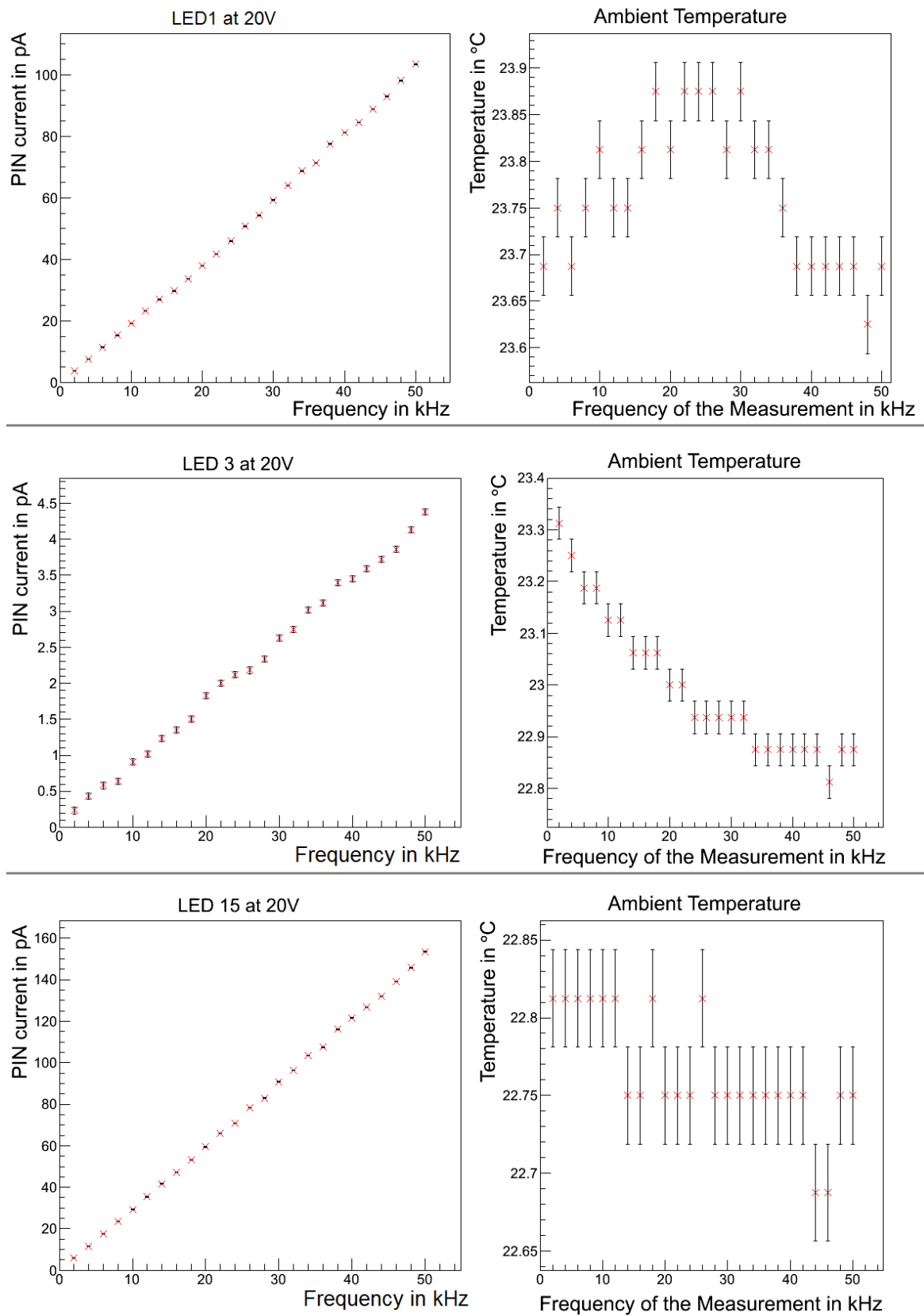
Figure 5.10: Measurement of the frequency dependence of the pulser at 20 V
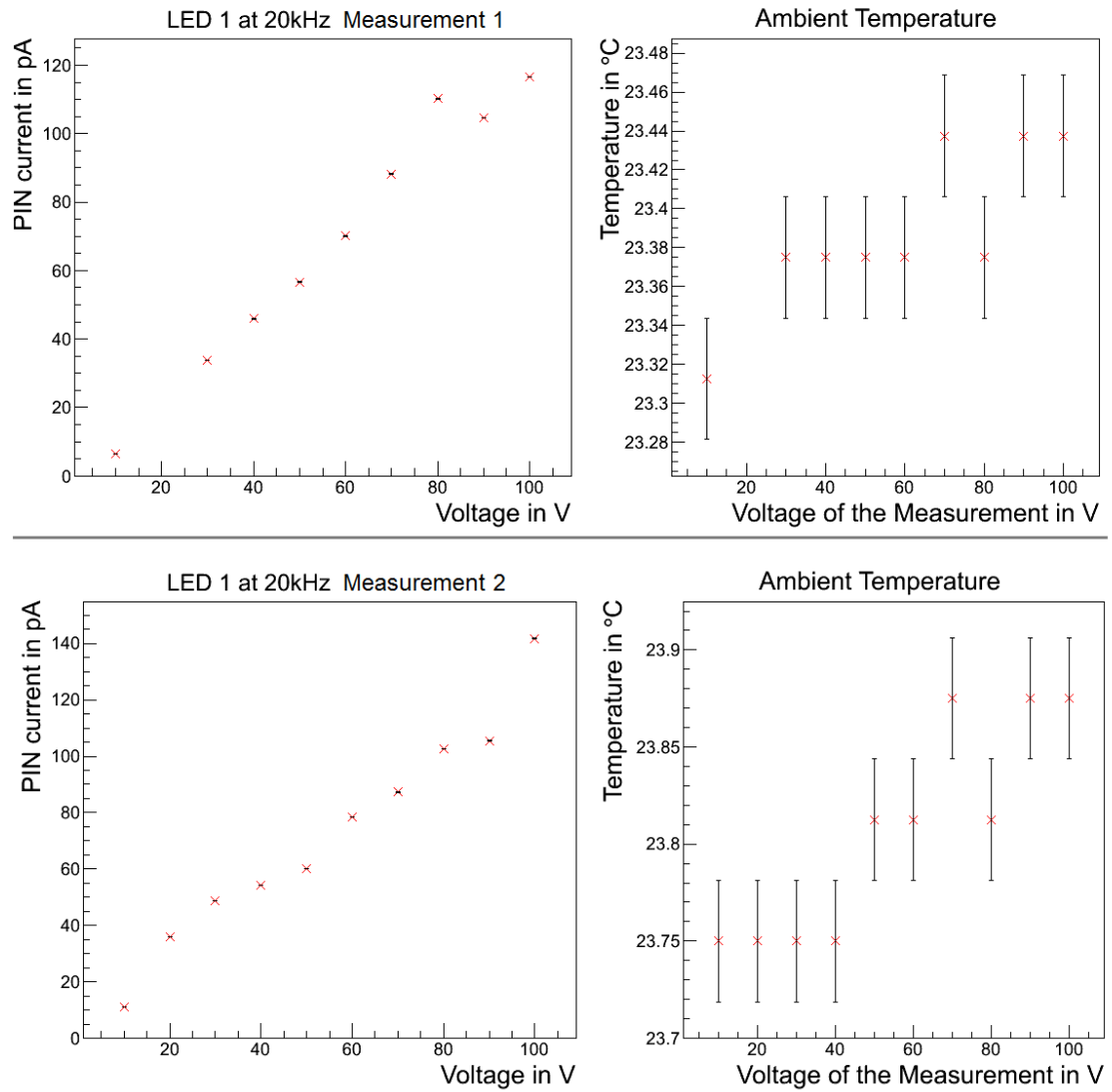
Figure 5.11: Two measurements of the voltage dependence of the pulser with LED 1 at 20 kHz
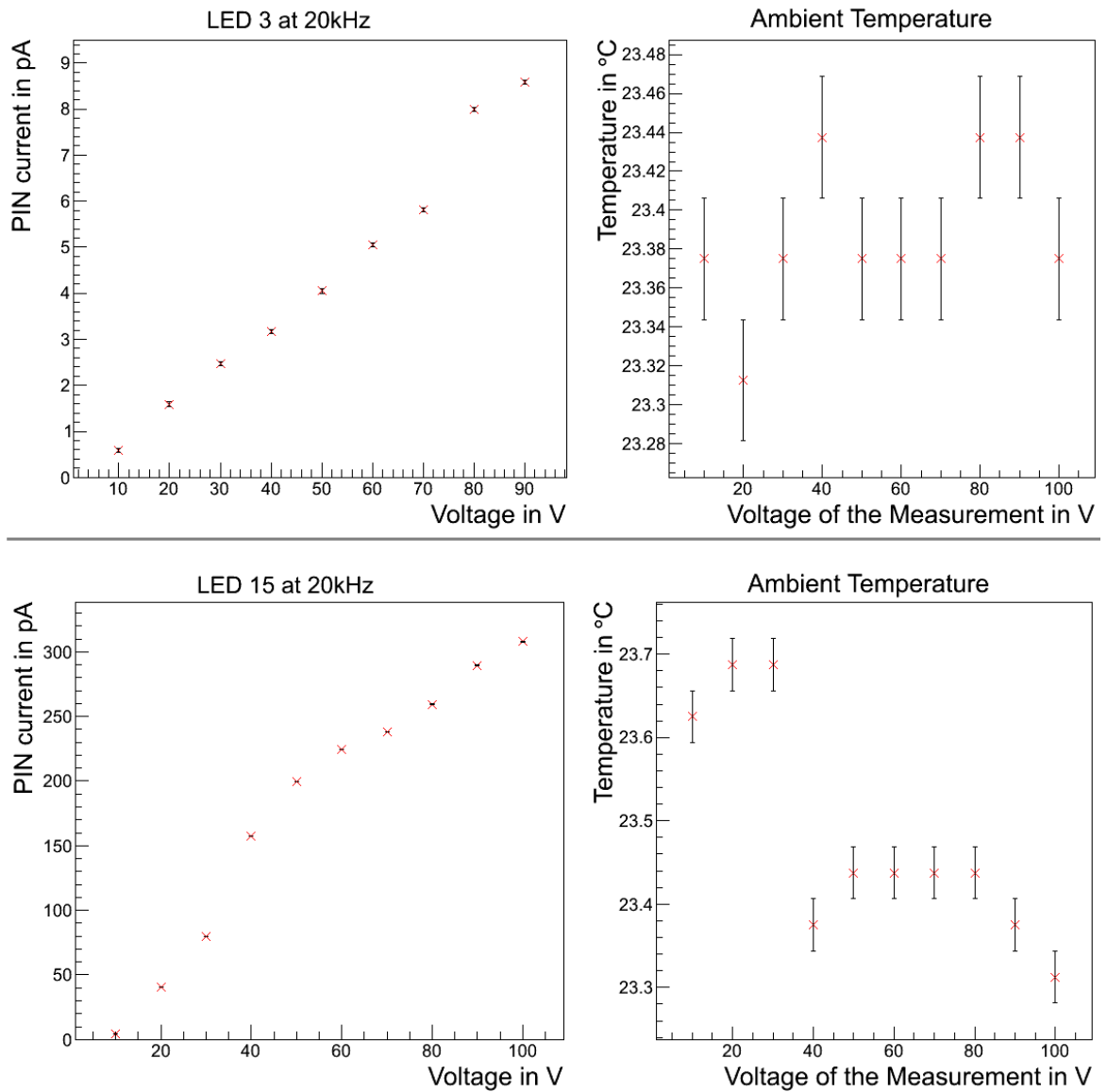
Figure 5.12: Measurements of the voltage dependence of the pulser with LED 3 and LED 15 at 20 kHz
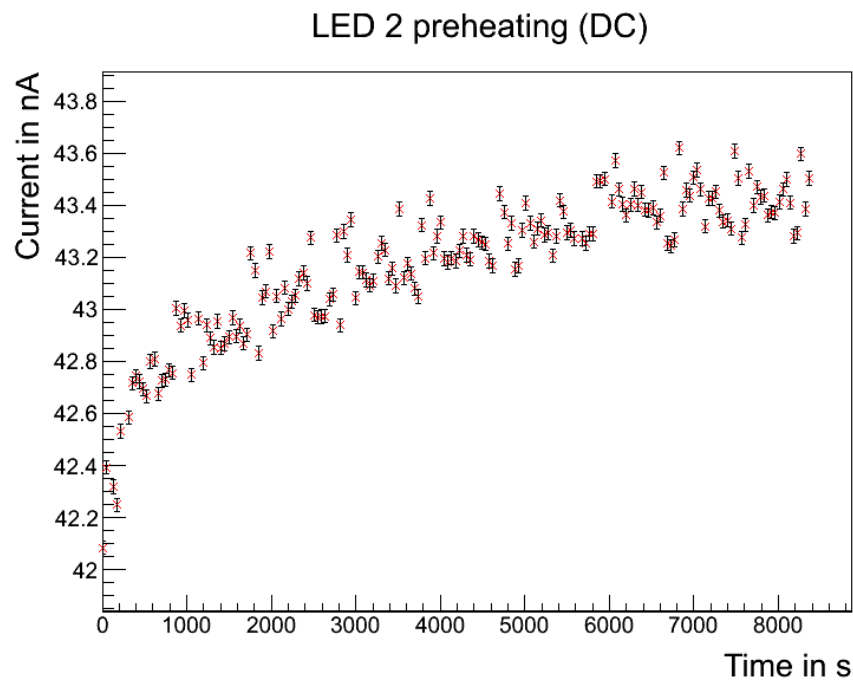
Figure 5.13: This measurement shows the fluctuation of the photocurrent after turning on the DC module. The adjusted current is is 20 mA
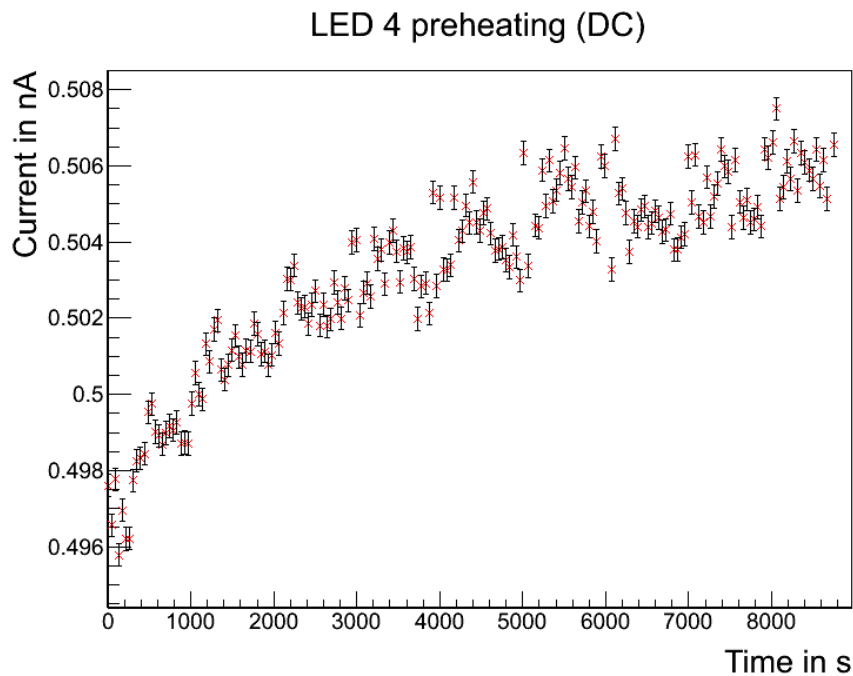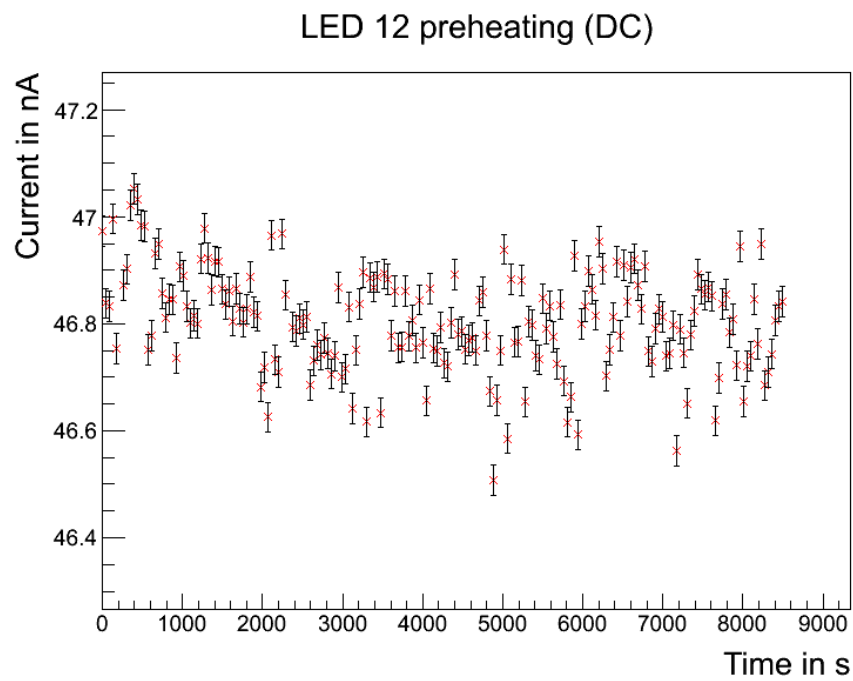

Figure 5.14: This measurement shows the fluctuation of the photocurrent after turning on the DC module. The adjusted current is is 20 mA

Figure 5.15: This measurement shows the fluctuation of the photocurrent after turning on the DC module. The adjusted current is is $20\,\mathrm{mA}$

6 Conclusion and Outlook

The silicon photomultiplier is a promising, very sensitive light detector. Many important experiments in the field of particle and astro-particle physics already use or are planning to use SiPMs. For most of them it is extremely important to have precisely characterized SiPMs, and thus the investigation in the properties of SiPMs is a vital project.

One of the most important properties to measure is the photon detection efficiency. In order to do so, the relative pde could be measured over a wide spectral range and then scaled to the results of a set of absolute pde measurements. The multipurpose light source has to provide the light fluxes for both types of measurements. Therefore, different types of DC-sources and pulsers have been tested and characterized. A modular concept has been developed which includes the best of the tested pulsers and a DC module for a constant light flux. In order to cover a wide spectral range from deep UV to red several types of LEDs have been characterized and implemented in the light source. Nevertheless, its modularity allows to further extend the light source's spectral range easily.

For the characterization of the multipurpose light source a calibrated reference detector, a PIN diode, has been commissioned. The measurement method for the PIN diode's photocurrent has been optimized to measure very low currents with a sub-pA precision. Therefore, the leakage current and the coupling of external noise have been minimized.

The characterizations of the multipurpose light source shows that it provides a constant light flux with peak to peak fluctuations smaller than 0.8% for relative pde measurements in a spectrum ranging from 350 nm to 700 nm as well as pulsed light (< 10 ns) in the range from 315 nm to 590 nm. The intensity of the light pulses ranges from single photons for the absolute pde measurements up to several thousand photons per pulse and mm^2 for studying the dynamic range of SiPMs. Moreover, the multipurpose light source is completely computer-controlled and thus is perfectly suitable for fully automated measurements.

When measuring the absolute pde the two main error sources will be the calibration of the PIN diode (5%) and inequalities in the light distribution by the optical set-up to the ports for PIN diode and the SiPM. In order to measure the pde one has to know the ratio of the light intensities at these two ports. Though this ratio can be measured with the PIN diode, it changes every time the device at one of the ports

is changed. The reason for this begins with mechanical production tolerances for example of the different apertures and ends with a changing orientation of the optical parts when changing the SiPM. The error on this is hard to estimate, and 10% seems to be an optimistic aim. The statistic error on the number of emitted photons is not that much of a problem as it can be reduced by multiple measurements. All in all an accuracy of 15% on the absolute pde measurement seems to be realistic. The relative pde measurement will be more precise as most of the errors in the ratio of the measured electrical currents through SiPM and PIN diode cancel and only the wavelength-dependent part of the errors remains.

The next step would be to do a full characterization of the multipurpose light source and find the optimal settings for SiPM measurements. Here a 'convenience' function which adjusts the light flux of the selected LED to a given number of photons is planned. This will be done by a program which readjusts the parameters for the light source due to the measured photocurrent. Finally one can measure the photon detection efficiency of various SiPMs in dependency of the parameters temperature and overvoltage.

Bibliography

[1] S. España and G. Tapias, *Performance Evaluation of SiPM Detectors for PET Imaging in the Presence of Magnetic Fields*, IEEE Nuclear Science Symposium Conference Record, (2008), pp. 3591–3595. 1

[2] D. Renker and E. Lorenz, *Advances in solid state photon detectors*, Journal of Instrumentation, 4, (2009), p. P04004. 1, 1.6

[3] H. Anderhub *et al.*, *FACT - The first Cherenkov telescope using a G-APD camera for TeV gamma-ray astronomy*, Nucl. Instrum. Meth. A, Volume 639, Issue 1, (2011), pp. 58–61. 1

[4] S. Assylbekov *et al.*, *The T2K ND280 Off-Axis Pi-Zero Detector*, Nucl. Instrum. Meth. A 686, (2012), pp. 48–63. 1

[5] E. Aprile and P. Cushman and K. Ni and P. Shagin, *Detection of Liquid Xenon Scintillation Light with a Silicon Photomultiplier*, Nucl.Instrum.Meth. A556, (2006), pp. 215–218. 1

[6] T. Niggemann *et al.*, *Proc. of 33th int. cosmic ray conf*, (2013). 1

[7] B. Beischer *et al.*, *A high-resolution scintillating fiber tracker with silicon photomultiplier array readout*, Nucl. Instrum. Meth. A Volume 622 and Issue 3, (2010), pp. 542–554. 1

[8] C. Heidemann, *Direkte Messung der Driftgeschwindigkeit im Gas der CMS-Myonenkammern mit VDC-Kammern*, diploma thesis RWTH Aachen, (2010). 1

[9] Yi Qianga, Carl Zorn, Fernando Barbosa, Elton Smith, *Radiation Hardness Tests of SiPMs for the JLab Hall D Barrel Calorimeter*, (2012). 1

[10] S. M. Sze and K. K. Ng, *Physics of semiconductor devices*, Wiley-Interscience, 2007. 1.1.1, 1.2, 1.1.2, 1.3, 3.3

[11] M. Lauscher, *Characterisation studies of silicon photomultipliers for the detection of fluorescence light from extensive air showers*, master thesis RWTH Aachen. 1.4, 1.2.2, 1.2.3

[12] W. G. Oldham, R. R. Samuelson and P. Antognetti, *Triggering phenomena in avalanche diodes*, IEEE Transactions on Electron Devices, 19, (1972), pp. 1056–1060. 1.4

[13] B. Glauss, *Optical Test Stand and SiPM characterisation studies*, master thesis RWTH Aachen, (2012). 1.5, 1.1.2, 2, 2.1

[14] K. Rajkanan, R. Singh, and J. Shewchun, *Absorption coefficient of silicon for solar cell calculations*, Solid-State Electronics, 22, (1979), pp. 793–795. 1.6

[15] M. Merschmeyer, *private communication*, (2013). 1.8

[16] S. Richer, *Conception of a test stand for Silicon Photomultipliers*, bachelor thesis RWTH Aachen, (2010). 2

[17] M. Lins, *Construction and testing of a tunable light source for characterisation of Silicon Photomultipliers*, 2010. 2

[18] Hamamatsu, *Si PIN photodiode S9195 Datasheet*, Hamamatsu. 2, 3, 3.4

[19] Keithley Instruments, *Keithlery instruments model 6485 picoammeter datasheet.* 2

[20] E. Fred Schubert, *Light-Emitting Diodes*, Cambridge University Press, 2006. 2.1, 4.2, 5.3

[21] P. Hallen, *Determination of the Recovery Time of Silicon Photomultipliers*, bachelor thesis RWTH Aachen, (2011). 2.3.1

[22] F. Scheuch, *Measurement and simulation of electrical properties of SiPM photon detectors*, master thesis RWTH Aachen, (2012). 2.3.1

[23] Keithley Instruments, *Series 2600B System SourceMeter Source-Measurement Unit (SMU) Instruments Datasheet.* 3, 3.4, 5.2

[24] Hamamatsu, *http://www.hamamatsu.com/jp/en/product/alpha/P/4103/S9195/index.html*, last checked October 2013. 3.1

[25] Hamamatsu, *Calibration datasheet S9195*, 2013. 3.2, 3.3

[26] Keithley Instruments, *Low Level Measurements Handbook 6th Edition*, 2004. 3.2

[27] U. Tietze and C. Schenk, *Halbleiter-Schaltungstechnik 12. Auflage*, Springer-Verlag, 2012. 3.4

[28] Ocean Optics, *http://www.oceanoptics.com/products/usb650uvvis.asp*, last checked November 2013. 4.2

Danksagung - Acknowledgements

Eidesstattliche Erklärung

Ich versichere, dass ich die Arbeit selbstständig verfasst und keine anderen als die angegebenen Quellen und Hilfsmittel benutzt sowie Zitate kenntlich gemacht habe.

Aachen, den 13.12.2013

———————————————

TIM ENZWEILER